MSc in Photonics

PHOTONICS**BCN**

Universitat Politècnica de Catalunya (UPC)
Universitat Autònoma de Barcelona (UAB)
Universitat de Barcelona (UB)
Institut de Ciències Fotòniques (ICFO)

http://www.photonicsbcn.eu

Master in Photonics

MASTER THESIS WORK

STRONG COUPLING OF ORGANIC MOLECULES TO A PLASMONIC NANO-ANTENNA CAVITY

Lander Gyssels

Supervised by Prof. Dr. Niek van Hulst, ICFO
Prof. Dr. Ir. Peter Bienstman, Ghent University

Presented on date 20th of July 2022

Registered at

Preface

I would like to thank several people who have helped me a lot through the process that lead to this thesis. Both my supervisors, Prof. Dr. Ir. Peter Bienstman at Ghent University and Prof. Dr. Niek F. van Hulst at UPC and ICFO have helped me a lot administratively and organizationally. Furthermore, I want to thank the complete Molecular Nanophotonics group at ICFO for all the help. Especially Monserrat Alvarez Ortiz for helping me getting started, all the information on the topic of my thesis and the fabrication of the samples, and Saurabh Borkar for his help with the setup and the measurements.

Permission for use of content

Lander Gyssels
20/06/2022

This master's dissertation is part of an exam. Any comments formulated by the assessment committee during the oral presentation of the master's dissertation are not included in this text.

Abstract

This work is the master thesis of Lander Gyssels, writen in order to obtain the academic degree of the European Master of Science in Photonics, in the academic year 2021-2022. This master thesis is supervised by Prof. Dr. Ir. Peter Bienstman at Ghent University and Prof. Dr. Niek F. van Hulst at UPC and the Institute of Photonic Sciences, ICFO.

The optical properties of molecules can be changed by the presence of a cavity [1]. If the cavity is resonant with a certain transition of the molecules, the molecules couple with the cavity. The coupling is characterized by the coupling strength g, which represents the rate of energy exchange [2]. When g is high enough, the exchange rate can overcome the losses of the cavity and the molecules and so-called strong coupling is achieved. The strongly coupled system has new states that can no longer be described by the properties of the 2 components alone. Achieving strong coupling is the goal of this thesis. Plasmonic nanocavities, or nanoantennas can confine light to volumes smaller than the diffraction limit. Rod antennas and dimer antennas, which consists of 2 rod antennas separated by a gap are of interest in this thesis. An interesting property of a dimer is that it can build up a high field strength in the gap, leading to an increase in g. The mode volume is pushed down to an estimated $20\,000\,\mathrm{nm}^3$, well below the diffraction limit. The length and gap size of the dimers is varied so the plasmonic resonance frequency matches the molecular resonance frequency. This process is backed up with FDTD simulations. The observed coupling strength g for rods is $0.106 \pm 0.017\,\mathrm{eV}$ and $0.116 \pm 0.014\,\mathrm{eV}$ for dimers with a molecular concentration of $195 \pm 48\,\mathrm{mM}$.

Keywords: plasmonics, nanocavity, coupling strength

Strong coupling of organic molecules to a plasmonic nano-antenna cavity

Lander Gyssels
Supervisors: Peter Bienstman, Niek F. van Hulst

20/06/2022

Abstract

Molecules placed in an optical cavity experience a change in the environment that leads to changes in their optical properties. If the cavity is resonant, molecules can couple to the cavity with a certain coupling strength g. When g surpasses a minimal value, molecules and the cavity form a strongly coupled system with states that are part light, part matter. Achieving strong coupling is therefore the goal of this thesis. In a plasmonic cavity, the mode volumes can become smaller than the diffraction limit, down to an estimated $20\,000\,\mathrm{nm}^3$ with Au nanoantennas in this thesis. The achieved coupling strength with Rhodamine 800 and dimer nanoantennas is $0.116 \pm 0.014\,\mathrm{eV}$ while the minimal value is $0.103 \pm 0.008\,\mathrm{eV}$ with a molecular concentration of $195 \pm 48\,\mathrm{mM}$.

Keywords: plasmonics, nanocavity, coupling strength

1 Introduction

The interaction between light and matter is often suppressed by their difference in size. Molecules are generally a lot smaller than the wavelength of the light they emit, leading to a low absorption and emission probability. Since the optical properties of molecules depend on the local density of states (LDOS) [1], they can be modified by external factors. Molecules can couple to a cavity if the resonance frequency matches the molecular resonance frequency. In this thesis, plasmonic nanoantennas are investigated. The geometry is varied to match the molecular resonance as to maximize the coupling. If the coupling is big enough, the molecules and the cavity form a strongly coupled system. The exchange of energy between the molecules and cavity is then faster than the losses and the system has new states that are part light, part matter [2]. Strongly coupled systems have several applications: ultralow-threshold and single molecule lasers [3, 4], light harvesting [5] and the creation and preservation of a qubit [6].

2 Theoretical background

Plasmonic nanocavities can confine light to mode volumes well below the diffraction limit, given by $V_m = (\lambda/2n)^3$ [7]. The small mode volume leads to a high field intensity. Especially if 2 structures are combined and separated by a gap, the field intensity reaches

high values in the gap. In this thesis, the investigated nanoantennas are rod-shaped nanoantennas and dimer nanoantennas made out of Au. A dimer consists of 2 rods with a gap in between. The 2 rods in the used dimers are always symmetric. Varying the geometry allows tuning of the plasmonic resonance frequency ω_{pl} to make the nanoantenna resonant with the molecular resonance frequency ω_{mol}. FDTD simulations show that longer lengths lead to a lower ω_{pl}, as well as smaller gaps. ω_{pl} also depends on the refractive index of the surrounding. In the presence of molecules, a natural shift towards lower frequencies is expected. ω_{pl} can be seen in the scattered field of the nanoantennas. The linewidth of the scattering cross section β_{pl} increases for longer nanoantennas and can also be seen in the scattered field [8].

The optical properties of interest are the molecular resonance frequency ω_{mol} and the decay rate Γ_{mol}. Both quantities are retrieved from absorbance measurements. The used molecules are Rhodamine 800, noted as LD800.

The interaction between the nanoantennas and the molecules is characterized by the coupling strength g and is defined as [2]

$$g = \sqrt{N}\boldsymbol{\mu} \cdot \boldsymbol{E},$$

with N the amount of molecules, $\boldsymbol{\mu}$ the transition dipole moment of the molecule and $\boldsymbol{E}$ the electric field. μ equals 4 D for LD800 [9]. g represents the rate of energy exchange between the nanoantenna and the molecules. 2 regimes are differentiated depending on the magnitude of g, weak coupling and strong coupling. The minimal value for strong coupling is [10]

$$g_{min} = \frac{\beta_{pl} + \Gamma_{mol}}{4}.$$

If g is smaller than $(\beta_{pl}+\Gamma_{mol})/4$, the system is in the weak coupling regime, where the nanoantenna enhances the decay rate of the molecules. The strong coupling regime, where g is bigger than $(\beta_{pl} + \Gamma_{mol})/4$, is of interest in this thesis. The strongly coupled system now has 2 different resonance frequencies, called the upper and lower polariton, separated by 2Ω. This is called Rabi splitting and Ω is the Rabi frequency [11]. Ω is also visible in the scattered field. The central frequency between the polaritons is given by $(\omega_{pl} + \omega_{mol})/2$. In experiments, Ω can be observed and g can be calculated from Ω if $\omega_{pl}, \omega_{mol}, \beta_{pl}$ and Γ_{mol} are known. If g is high enough for strong coupling but ω_{pl} is detuned from ω_{mol}, the 2 polaritons coincide with ω_{pl} and ω_{mol}. This is called anticrossing [12].

3 Methods

The nanoantennas are fabricated with EBL and Au evaporation through a liftoff process after a 9 nm layer of ITO is applied to the glass substrate to enhance the adhesion of Au to glass. The nanoantennas are 50 nm high and wide. The length of the nanoantennas varies from 60 to 150 nm in steps of 10 nm. It has to be mentioned that if a dimer is said to be of a certain length and with a certain gap, it means that the rods have that length and they are separated by that gap. There are arrays of nanoantennas with an intended gap of 25 and of 30 nm. A solution of LD800 in ethanol is added to the sample and spin coated after the sole nanoantennas are measured. The spin coating results in a layer of 20 to 25 nm.

The used setup is a wide-field illumination, dark-field microscopy setup to detect the scattered field. The spectrum is made flat by splitting the spectral components of a pulsed laser (SuperK Extereme EXR-20

by NKT Photonics) with a repetition rate of 78 MHz onto an SLM. A voltage mask is created that results in a flat spectrum. The coherence of the beam is reduced to reduce speckles in the beam. This is done by reflecting the beam by 2 galvanometer mirrors and sending the beam through a multimode fiber with a 100 µm core. The sample is illuminated through an oil-immersion objective (Nikon lambda series, NA 1.4, magnification of 60). A part of the scattered light travels back through the same objective past a dark-field mask and is focused onto an EMCCD camera (ImagEM C9100-13 by Hamamatsu). Also an effective phase modulation is applied to the SLM. The following equation is used [13].

$$I(\omega, t) = |\cos((\omega - \omega_0)t)|^2,$$

where I is the reflected intensity in function of frequency ω that is incident on the pixel of the SLM and ω_0 the rotating frame frequency.

4 Results

With UV-VIS equipment, the absorbance of LD800 is measured. The absorbance spectrum shows a peak at $\omega_{mol} = 1.82\,\text{eV}$ with a linewidth of $\Gamma_{mol} = 0.116\,\text{eV}$. There is another peak at 1.99 eV but this peak is not of interest because of its lower amplitude. The absorbance spectrum is plotted on the left hand side of Figure 2.

In order to determine ω_{pl} and β_{pl}, the scattered field from nanoantennas without molecules is measured. First, the rods are measured since only the length is varied for these nanoantennas. An offset in ω_{pl} of $0.097 \pm 0.023\,\text{eV}$ compared to the simulated values is observed, as shown in Figure 1. β_{pl} is $0.048 \pm 0.030\,\text{eV}$ higher than the simulated values. This is the result of surface roughness of the nanoantennas. For the dimers, ω_{pl} and β_{pl} follow the same trend as predicted numerically, but with more variation. From the shift of ω_{pl} from ω_{pl} of the rod, an estimate can be made about the gap. For the arrays with an intended gap of 25 nm, the estimated gap ranges from 8 to 20 nm, while for the 30 nm arrays the range is from 13 to 27 nm. The mode volume V_m of a dimer nanoantenna can be approximated by the volume in the gap [14]. The 8 nm gap nanoantenna therefore has a mode volume of $20\,000\,\text{nm}^3$.

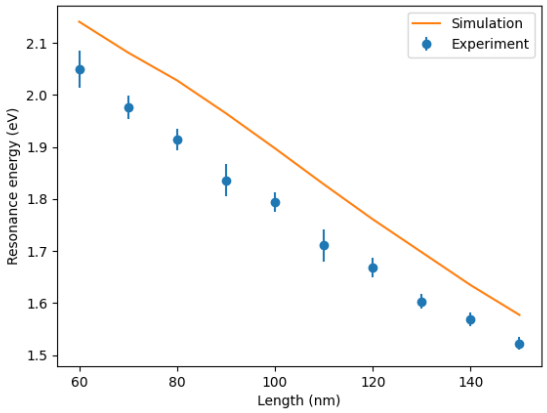

Figure 1: comparison of experimental and theoretical values of ω_{pl} for rod nanoantennas.

The intended concentration of LD800 in the ethanol solution is 150 mM. In the experiment, both the Rabi splitting and the anticrossing behaviour have to be observed in order to have strong coupling. Even though dimers are more suitable for strong coupling because of the high field intensity in the gap, strong coupling has been observed in both rods and dimers. For the rods with strong coupling, the calculated g from the observed Ω is $0.106 \pm 0.017\,\text{eV}$, while $(\beta_{pl} + \Gamma_{mol})/4$ is $0.094 \pm 0.011\,\text{eV}$. The rods that achieved strong coupling have a length of 90 nm.

Depending on the gap size, different

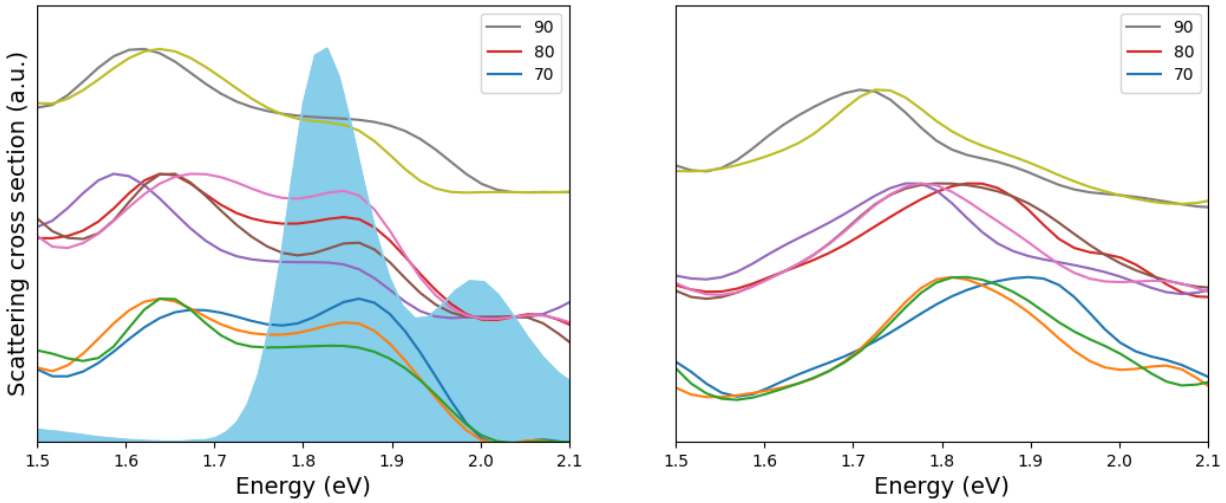

Figure 2: Dimers in a 30 nm gap array where strong coupling is observed. The lower band has a length of 70 nm, the middle one of 80 nm and the upper one of 90 nm. The scattering cross sections on the left are of nanoantennas with molecules and the absorbance of LD800 is added as a reference. The scattering cross section on the right correspond to the same nanoantennas without molecules.

lengths of dimers match the molecular resonance frequency ω_{mol}. For the arrays with intended gap 25 nm, the 60 nm dimers exhibit strong coupling. For the 30 nm arrays, 70 nm dimers are more likely to achieve strong coupling. The achieved coupling strength is 0.116 ± 0.014 eV, with minimum values of 0.103 ± 0.008 eV. In 25 nm gap arrays, ω_{pl} is often too small to match ω_{mol}, but the electric field is stronger because of the smaller gaps. Because of the mismatch, 65% of the observed strong coupling were in 30 nm gap arrays.

The longer nanoantennas that do not exhibit Rabi splitting because of their resonance mismatch, such as the 90 nm dimers in Figure 2, are used to determine the shift of ω_{pl} due to the presence of molecules and to confirm anticrossing. For the dimers, the mode volume can be estimated and therefore, the amount of coupled molecules can be calculated. Under the assumption that the coupling molecules are all located inside the gap and μ is parallel to E, the concentration can be estimated. The molecular concentration is 195 ± 48 mM. Given the assumptions, this is only a rough estimate.

The obtained values for g are only slightly higher for dimers than for rods. Also β_{pl} is generally smaller for rods than for dimers, lowering the minimal strong coupling value. Still, strong coupling is 13% more likely to happen at dimers than at rods in the performed experiments.

5 Conclusions

The geometry of plasmonic nanoantennas is varied so that its resonance frequency ω_{pl} matches the molecular resonance frequency ω_{mol}. Dimers, consisting of 2 identical rods separated by a gap, have a lower ω_{pl} for higher lengths and for smaller gaps. Matching

the resonance frequency maximizes the coupling strength g between molecules and the nanoantenna. If g surpasses $(\beta_{pl} + \Gamma_{mol})/4$, strong coupling is achieved. β_{pl} and Γ_{mol} represent the losses of the nanoantenna and the molecules respectively and is detected by the presence of 2 new states, the lower and upper polariton.

ω_{mol} and Γ_{mol} are determined by absorbance measurements and equal 1.82 eV and 0.116 eV respectively. The fabricated nanoantennas have a lower resonance frequency compared to the FDTD simulations. The offset is 0.097 ± 0.023 eV. For dimers with an intended gap of 25 nm, the gap ranges from 8 to 20 nm. For 30 nm gap dimers, the range is from 13 to 27 nm.

With 80 and 90 nm rods, strong coupling is achieved with a coupling strength g of 0.106 ± 0.017 eV, while the minimal value is 0.094 ± 0.011 eV. With 60 and 70 nm dimers, the achieved coupling strength is 0.116 ± 0.014 eV with a minimal value of 0.103 ± 0.008 eV. The molecular concentration of LD800 is 195 ± 48 mM. 65% of the observed strong coupling happened with 30 nm dimers. Dimers are also 13% more likely to achieve strong coupling than rods.

6 References

[1] J M Zhang and Y Liu. Fermi's golden rule: its derivation and breakdown by an ideal model. *European Journal of Physics*, 37(6):065406, oct 2016.

[2] James T Hugall, Anshuman Singh, and Niek F van Hulst. Plasmonic cavity coupling. *Acs Photonics*, 5(1):43–53, 2018.

[3] Perry R Rice and HJ Carmichael. Photon statistics of a cavity-qed laser: A comment on the laser–phase-transition analogy. *Physical Review A*, 50(5):4318, 1994.

[4] Jason McKeever, Andreea Boca, A David Boozer, Joseph R Buck, and H Jeff Kimble. Experimental realization of a one-atom laser in the regime of strong coupling. *Nature*, 425(6955):268–271, 2003.

[5] Changlong Wang and Didier Astruc. Nanogold plasmonic photocatalysis for organic synthesis and clean energy conversion. *Chemical Society Reviews*, 43(20):7188–7216, 2014.

[6] Tatjana Wilk, Simon C Webster, Axel Kuhn, and Gerhard Rempe. Single-atom single-photon quantum interface. *Science*, 317(5837):488–490, 2007.

[7] Dmitri K Gramotnev and Sergey I Bozhevolnyi. Plasmonics beyond the diffraction limit. *Nature photonics*, 4(2):83–91, 2010.

[8] Min Hu, Carolina Novo, Alison Funston, Haining Wang, Hristina Staleva, Shengli Zou, Paul Mulvaney, Younan Xia, and Gregory V Hartland. Dark-field microscopy studies of single metal nanoparticles: understanding the factors that influence the linewidth of the localized surface plasmon resonance. *Journal of materials chemistry*, 18(17):1949–1960, 2008.

[9] Denis G Baranov, Martin Wersall, Jorge Cuadra, Tomasz J Antosiewicz, and Timur Shegai. Novel nanostructures and materials for strong light–matter interactions. *Acs Photonics*, 5(1):24–42, 2018.

[10] Elad Eizner, Ori Avayu, Ran Ditcovski, and Tal Ellenbogen. Aluminum

nanoantenna complexes for strong coupling between excitons and localized surface plasmons. *Nano letters*, 15(9):6215–6221, 2015.

[11] Peter L Knight and Peter W Milonni. The rabi frequency in optical spectra. *Physics Reports*, 66(2):21–107, 1980.

[12] Lukas Novotny. Strong coupling, energy splitting, and level crossings: A classical perspective. *American Journal of Physics*, 78(11):1199–1202, 2010.

[13] Matz Liebel, Costanza Toninelli, and Niek F van Hulst. Room-temperature ultrafast nonlinear spectroscopy of a single molecule. *Nature Photonics*, 12(1):45–49, 2018.

[14] Stefan A Maier. Effective mode volume of nanoscale plasmon cavities. *Optical and Quantum Electronics*, 38(1):257–267, 2006.

Table of contents

1 Introduction

Light-matter interaction is at the core of every photonic technology. The interaction between light and molecules is often suppressed by the difference in size between molecules and the light they emit and absorb. Molecular dimensions are up to a few nanometers, while they emit in the visible region of the electromagnetic spectrum. This size mismatch causes the probability of emission and absorption of light to be very small [3]. This inefficiency limits the use of single molecule or small amounts of molecules in technologies. However, it is proven that the optical properties of atoms are not completely intrinsic, they can be modified by external factors. Fermi's golden rule says that the transition probability per unit of time is dependent on the Local Density of States (LDOS) of the energy of the final state [1]. The LDOS can be changed by changing the local photonic environment around the emitter, for example by placing the molecule in a resonant cavity [2]. This allows controlling optical properties, especially increasing or decreasing the absorption and emission cross sections and emission rates.

In metallic substances, there are a lot of free electrons. When light is incident on metallic substances, the electrons start to oscillate with the same frequency as the incoming light. The collective electron oscillations are called plasmons [4]. The oscillations of the electrons will re-emit light with the same frequency. Plasmons become particularly interesting in metallic nanoparticles. The size of the nanoparticle determines which plasmons can exist in the nanoparticle and therefore also which wavelengths of light will be absorbed. The energy corresponding to that wavelength is the resonance energy. Also the shape of the nanoparticle has a big impact on the absorption. When analyzing the electron oscillations in the nanoparticle, it can be seen that the emission of light is strongly localized at some hotspots. The localization of the emitted modes can be well below the diffraction limit of dielectric structures. The discovery of sub-wavelength localization gives rise to a series of applications, since this is not possible with dielectric materials. Low-threshold lasers [5], photodetectors [6] and cancer treatments [7] are a couple of examples.

If molecules are placed inside a hotspot of a metallic nanoparticle, the interaction between the light and the molecule can be severely increased because of the high intensity and strong localization of the light. For the strongly confined modes, the LDOS is very high, leading to a stronger absorption and emission of photons and a higher emission rate. The coupling is described with one parameter: the coupling strength g. The interaction is split into 2 regimes, depending on the coupling strength: weak coupling and strong coupling. In the weak coupling regime, sometimes also called bad-cavity regime, the emission of photons by the molecules is changed. The presence of the metallic particle decreases the lifetime of an electron in an excited state by increasing the LDOS. In the strong coupling regime, the molecules and the nanoparticle have to be described as a single system that has properties that are distinctively different than the 2 isolated systems. The system now has properties that are part light, part matter [8, 9]. The exchange of energy between molecule and plasmons is efficient, also called coherent. Both the weak and strong coupling regime have caught the attention of scientists and both have applications. Single photon sources are the most common applications for weak coupling [10]. Strong coupling has its applications is

quantum information [11] and light harvesting [12, 13] to name a few.

Several factors have to be taken into account for reaching strong coupling. On the one hand, there are the molecular optical properties. Especially the transition dipole moment and the absorption energy are important. On the other hand, there are the properties of the metallic or plasmonic nanoparticle. The absorption energy and the mode volume are key factors. For strong coupling to happen, the strong coupling condition needs to be fulfilled: the energy exchange betweens plasmons and molecule needs to be faster than the losses of the system.

In Section 2, a theoretical explanation will be given for everything that is mentioned in this Section: the molecular properties, the plasmonic properties and the interaction. Then, in Section 3, numerical simulations are carried out and will be discussed to confirm the theory, and later to compare with the measurements. Section 4 gives the fabrication process, measurement setup and data analysis method and the measurements will be discussed in Section 5. Finally, this thesis will be ended with the conclusions in Section 6.

2 Theoretical background

To understand coupling between plasmonic nanoantennas and molecules, the plasmonic properties of the nanoantenna, the molecular properties and the interaction between the 2 have to be understood. All 3 parts will be discussed in this section. First, the Drude model for metals will be given, to be applied to nanoantennas. Then, 2 different types of nanoantennas and their shape will be discussed since the type and shape have a severe impact on the resonances and coupling strength. Subsequently, the Lorentz model is discussed and applied to the emitters in a similar way. The interaction of the molecules with the fields and how this effects the properties of the system will be discussed and finally, 2 different regimes for coupling, weak and strong coupling, will be discussed with its conditions, properties and applications.

2.1 Plasmonic nanoantennas

2.1.1 Drude model

All the optical properties of a metal are included in the permittivity $\epsilon(\omega)$ [14]. $\epsilon(\omega)$ is a complex function of the optical frequency ω. The real part, called ϵ_R in this thesis, determines the refractive index of the medium, while the imaginary part, ϵ_I, describes the attenuation of light in the medium. The Drude model is a classical model that estimates the permittivity ϵ [15], i.e. it considers electrons moving classically in a classical electric field. The incident electric field will cause a force acting on the electrons. According to Newton's equations of motion, the electrons have to satisfy

$$m\frac{d^2\boldsymbol{x}}{dt^2} + \gamma m\frac{d\boldsymbol{x}}{dt} = e\boldsymbol{E}, \tag{1}$$

with m and e the mass and negative charge of the electron, γ the damping of the motion and $\boldsymbol{E}$ the incident electric field[1]. $\boldsymbol{x}$ is the displacement of the electron with respect to the nucleus. Note that no restoring force is included in the equation, meaning this is a description of a free electron. Solving this equation in the frequency domain gives

$$\boldsymbol{x}(\omega) = \frac{-e}{m(\omega^2 + i\gamma\omega)}\boldsymbol{E}(\omega). \tag{2}$$

The displacement of the electron creates a dipole moment, defined as

$$\boldsymbol{\mu}(\omega) = -e\boldsymbol{x}(\omega), \tag{3}$$

and can be written as

$$\boldsymbol{\mu}(\omega) = \frac{e^2}{m(\omega^2 + i\gamma\omega)}\boldsymbol{E}(\omega). \tag{4}$$

The dipole moment is indicated with a white arrow in Figure 1 [5]. The proportionality factor between $\boldsymbol{\mu}(\omega)$ and $\boldsymbol{E}(\omega)$ is called the atomic polarizability, and is noted as $\alpha(\omega)$.

[1] Physical quantities in bold represent vectors.

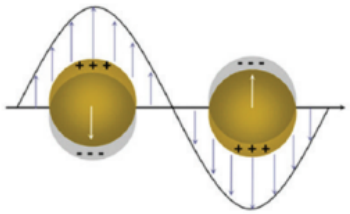

Figure 1: Collective oscillations of free electrons

Now, the macroscopic polarization $\boldsymbol{P}$ is defined as

$$\boldsymbol{P}(\omega) = N\boldsymbol{\mu}(\omega), \tag{5}$$

N being the density of atoms. The macroscopic polarization $\boldsymbol{P}$ is proportional to the applied electric field $\boldsymbol{E}$.

$$\boldsymbol{P}(\omega) = \epsilon_0 \chi_e(\omega)\boldsymbol{E}(\omega), \tag{6}$$

with ϵ_0 the permittivity of vacuum. From the constitutive relations, it is known that $\epsilon = 1 + \chi_e$. This gives following expression for the permittivity

$$\epsilon(\omega) = 1 - \frac{\omega_p^2}{\omega^2 + i\gamma\omega}, \tag{7}$$

with $\omega_p = Ne^2/\epsilon_0 m$ the so-called plasma frequency. For the atomic polarizability, the following expression holds

$$\alpha(\omega) = \frac{-e^2}{m(\omega^2 + i\gamma\omega)}. \tag{8}$$

It can be said that α is a microscopic property, while ϵ is macroscopic since it is dependent on the molecular density N. By looking at the general expression for ϵ, some remarks can be made. For low frequencies, i.e. $\omega < \omega_p$, ϵ_R is negative. This means that the fields will only penetrate the metal to a very short distance, or the material is highly reflective. The distance light can penetrate into the material is called the skin depth δ. For high frequencies, $\omega > \omega_p$, ϵ_I is very small, leading to a very low absorption. At the same time, ϵ_R approaches 1, corresponding to a very low reflectivity. This makes the material transparent. In this thesis however, only values of ω smaller than ω_p are relevant. The complex refractive index $n = n_R + in_I$ is completely determined by the permittivity by the equation $n = \sqrt{\epsilon}$. This equation can be separated for the real and imaginary part of n

$$\begin{aligned} n_R &= \sqrt{\frac{\sqrt{\epsilon_R^2 + \epsilon_I^2} + \epsilon_R}{2}} \\ n_I &= \sqrt{\frac{\sqrt{\epsilon_R^2 + \epsilon_I^2} - \epsilon_R}{2}}, \end{aligned} \tag{9}$$

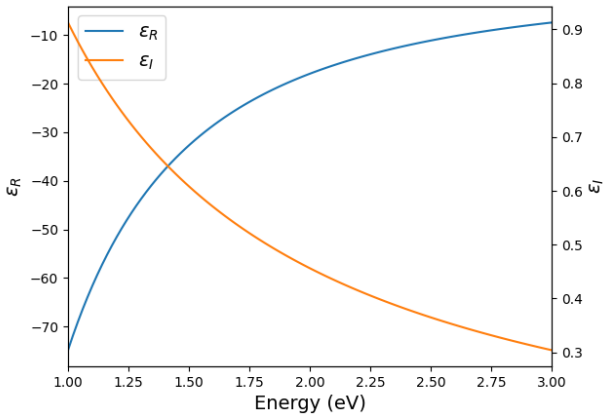

Figure 2: Theoretical prediction of the permittivity of Au

or the other way around when the refractive index is known

$$\begin{aligned} \epsilon_R &= n_R^2 - n_I^2 \\ \epsilon_I &= 2 n_R n_I. \end{aligned} \tag{10}$$

Moreover, the real and imaginary part of the refractive index n are related to each other through the Kramers-Kronig equations [16].

In this thesis, the nanoantennas are made out of gold (Au). For ω_p, the value 8.71 eV is used, for γ 83.1 eV [2] [17]. 8.71 eV corresponds to a wavelength of 142.3 nm, in the UV region.The theoretical estimation for ϵ is plotted in Figure 2 with the mentioned values. For ϵ_R, the damping γ is ignored, since this is only relevant for the losses, described by ϵ_I. This approach is often used in literature [18]. The skin depth δ of Au varies from 25 nm to 28 nm between the frequencies 1.5 eV and 2.1 eV [19]. Silver (Ag), copper (Cu) and aluminum (Al) are also commonly used for nanoantennas, but Au nanoantennas have less oxidation over time [20] and therefore degrade less.

2.1.2 Nanoantennas

2 shapes of nanoantennas will be discussed. The first one is the rod-shaped antenna, the second one is called a dimer antenna. A dimer antenna consists of 2 rod antennas, separated by a gap. Rods can be described analytically, dimers not completely. However, a lot of the theoretical insight from rods can be transferred to the dimers and a qualitative description can be given for dimers.

The shape of the rod antennas is characterized by 3 parameters: the length, the cross section area and the radius of curvature at the edges. The resonance frequency is determined

[2]Note that in this thesis, frequencies are always expressed in the energy units, here eV. The conversion is $E = \hbar\omega$.

by these 3 shape parameters and the permittivity $\epsilon(\omega)$. Since the range of frequencies in this thesis is around the visible range, i.e. frequencies well below ω_p, ϵ_R will always be negative. The nanoantennas are surrounded by air and the molecules, which all have a positive ϵ_R, allowing light to propagate. So when light is incident on the nanoantennas, there is a very low penetration in the nanoantennas. As a result, the plasmons will be localized at the surface of the nanoantennas. These plasmons are called localized surface plasmons (LSP). Because the dimensions of the nanoantennas are smaller than the wavelength of their resonant light (see Section 3), their shape will play a big role in their resonance frequency. The polarizability α is therefore dependent on the shape of the nanoantenna, and the direction of the electric field. Rod antennas can be approximated as ellipsoidal particle, for which an analytical description exists. The polarizability of an ellipsoidal nanoparticle along an axis i can be written as [21]

$$\alpha_i(\omega) = \frac{4}{3}\pi a_i \frac{\epsilon(\omega) - \epsilon_m}{\epsilon_m + L_i(\epsilon(\omega) - \epsilon_m)}. \tag{11}$$

ϵ_m is the permittivity of the surrounding medium, a_i is the semi-axis of the ellipsoid, L_i the geometrical form factor. It is clear that the polarizability is dependent on the direction of the applied field because of the dependence on L_i and a_i. As a result, the resonance frequency is different in different directions. The factor L_i becomes smaller for longer lengths of the ellipoid. To calculate the localized surface plasmon resonance (LSPR), γ can be neglected. The physical interpretation of this is that at resonance, the damping is minimal. From Equation 7, it can be seen that ϵ then reduces to $1 - \omega_p^2/\omega^2$. Also at the resonance, the polarizability α should be maximal. This happens when the denominator of Equation 11 approaches zero. the result is

$$\omega_{pl} = \frac{\omega_p}{\sqrt{1 + \epsilon_m(\frac{1}{L_i} - 1)}}, \tag{12}$$

where ω_{pl} is the LSPR. Since L_i is smaller for longer lengths, ω_{pl} is lower for longer nanoantennas. It can be concluded that the LSPR is dependent on material properties (ω_p), the surrounding environment (ϵ_m), the shape of the nanoantenna (L_i) and the direction of the electric field or the polarization. This frequency is the frequency of the fundamental mode in the nanoantenna, or the dipole. Other modes can also exist in nanoantennas due to contribution of quadrupoles and other higher order charge configurations [22]. These modes are not considered in this thesis. An important observation is that nanoantennas have a different resonance energy when they are completely surrounded by air, or when surrounded by molecules. If there are molecules present, ϵ_m is higher than for air. As a result, the resonance energy is lower. When light with the same frequency of the LSPR is incident on the nanoantenna, it will excite the plasmons most efficiently. Since plasmons are oscillations of charged electrons, they will re-emit light. The strongest re-emission is not at the LSPR because completely neglecting the damping of the oscillations is a too crude approximation. When looking at the near field, i.e. the field in close proximity of the nanoantenna, the frequency of resonance will be lower due to the damping. Instead of using γ, which is a microscopic parameter, the macroscopic parameter β_{pl} is used. The frequency of resonance

in the near field is given by

$$\omega_{nf} = \sqrt{\omega_{pl}^2 - \frac{\beta_{pl}^2}{2}}. \tag{13}$$

However, in this thesis, the measurements are done in the far field. In the far field and in the scattered field, the frequency of resonance remains ω_{pl} [23, 24]. Still, β_{pl} stays an important factor to achieve strong coupling, as will be discussed later. β_{pl} can also be retrieved from experiments, as it is the full width at half maximum (FWHM), also called linewidth, of the scattering cross section of the nanoantenna. The scattering cross section is defined as the total power scattered in all directions divided by the incident power flux [25] and is normalized for the spectrum of the source. Off-resonant light is also scattered, but with a smaller amplitude. This off-resonant scattering is stronger for light with a higher frequency and the amplitude scales with ω^4. This phenomenon is called Mie scattering and is valid for particles with dimensions smaller than the wavelength of their resonant light [26].

The re-emission of light is not the same in every position in the nanoantenna. In some spot the density of LSP's is larger. This results in a higher intensity of emitted light. These areas are called hotspots. For rod antennas, the hotspots are known to be at the edges and are stronger if the dipole along the long side of the rod is excited[27].

A dimer is essentially 2 rod-shaped nanoantennas separated by a gap d. All the aforementioned things are still valid for the separate rods, but the complete nanoantenna has different properties. In this thesis, only symmetrical nanoantennas are examined, meaning they consist of 2 identical rods. The optical properties of dimers are therefore only dependent on the geometrical parameters of the rods, the gap and the permittivity $\epsilon(\omega)$. In order to avoid confusion, it has to be mentioned that if a dimer is said to be of length L and gap d, it consists of 2 rods of length L, separated by a gap d. A dimer can not completely be described analytically. However, the resonance frequency of dimer shifts in the same way as rods: lower LSPR for longer dimers. Again, the polarization is an important factor for the resonance. The highest intensity in the far field is still the resonance frequency, while the near field resonance frequency is reduced according to Equation 13. γ is a microscopic parameter that is constant regardless of the shape of an nanoantenna. β_{pl} is its macroscopic counterpart and has different values for rods and dimers.

An estimation of the resonance frequency of a dimer can be done by considering mode hybridization [28, 29]. When 2 rods are in close proximity of each other, their modes will interfere with each other and they will form a system of 2 hybrid modes. The modes of the single rods are the same since only symmetric dimers are considered. This results in a symmetric splitting of the hybrid modes with respect to the single mode. The mode with the lower frequency is called the bonding mode, the one with the higher frequency the antibonding mode. A schematic representation of these 2 modes is shown is Figure 3. These hybrid modes are the results of the relative orientation of the dipole in the 2 rods. The orientation can be parallel, where the positive charge of one rod faces the negative charge of the other rod. This way, the dipoles in the 2 rods are weakened and the resonance energy is lowered. This corresponds to the binding mode. In a similar way, the dipoles can be antiparallel,

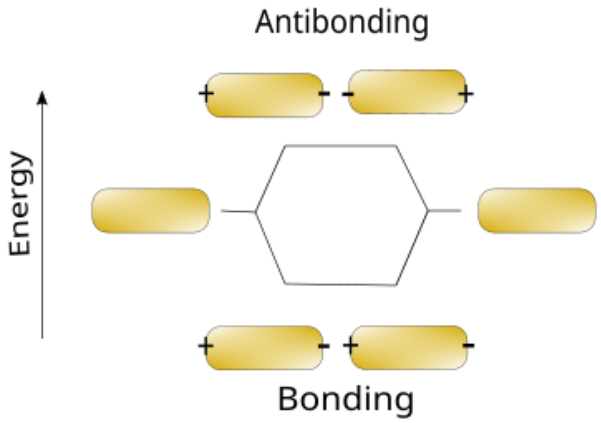

Figure 3: Mode hybridization in a dimer antenna

identical charges facing each other. The dipole moments in the rods are enhanced and the resonance frequency is higher. Since the parallel configuration is energywise more favourable, it has a much stronger field intensity in the gap. The size of the gap determines how strong the shift is. If the gap is smaller, the dipoles are closer to each other and the interaction between the 2 modes is stronger, leading to a higher shift and therefore a lower resonance frequency of the bonding mode.

Even tought the system has 2 modes, the antibonding mode will not appear in the far field. Only the near field will show its existence, but with a much lower magnitude [29]. The antibonding is therefore no longer of interest in this thesis and the intention is to tune the bonding mode to the molecular resonance frequency.

A qualitative description for the resonance frequency of a dimer exists and an estimate can be made, but the exact values for ω_{pl} and β_{pl} have to come from numerical simulations, as will be done in Section 3.

The reason dimer antennas are a popular choice for coupling with molecules, is their high field intensity at the hotspots. The hotspots of rods are at their edges, so combining 2 rods and overlapping their hotspots results in a high field intensity. The gap between the rods can be made very small, creating a small mode volume, well below the diffraction limit that dielectric cavities have [30, 31]. This is a property that makes dimer antennas desirable for interaction with molecules, as will be discussed below in Section 2.3.

Note that in Figure 3 the dipole along the long side is excited, i.e. the polarization of an incident field is parallel to the nanoantenna. If the field is perpendicular to the nanoantennas, the dipole along the short side will be excited. In that case, the dipoles in the 2 rods don't interfere with each other and the dimer acts as a rod and the resonance frequency is determined by the width of the nanoantenna only. Since the gap has no influence then, this excitation is not of interest. To take advantage of the gap and its high field intensity, the dipole along the long length is excited and the polarization of the field in the gap is then

parallel to the nanoantenna.

2.2 Molecules

The light that is emitted by molecules can excite plasmons in the nanoantennas. These plasmons will re-emit light that can be absorbed by the molecules. A thorough discussion of this back-and-forth emission and absorption will be given in Section 2.3. However, this means that it is important to know the optical properties of the molecules, here also called emitters. The Drude model can be generalized for dielectric media and is then called the Lorentz model [32]. The Lorentz model will be discussed here since the molecules that are supposed to couple to the nanoantennas are a dielectric medium. Since the permittivity contains all the optical information, including emission and absorption, it is useful to give a theoretical model for the molecules. Equation 1 needs to be modified since the electrons in a dielectric are not free. This is modelled by including a binding force $-K\boldsymbol{x}$, K being the force constant. The oscillations of the electrons are damped in a similar way as for metals, but here Γ_{mol} represents the emission rate or decay rate of the emitter. This way, a quantum mechanical phenomenon is included in a classical model.

$$m\frac{d^2\boldsymbol{x}}{dt^2} + m\Gamma_{mol}\frac{d\boldsymbol{x}}{dt} + K\boldsymbol{x} = e\boldsymbol{E}. \tag{14}$$

Γ_{mol} is similar to β_{pl}. It is the FWHM of the emission spectrum of a molecule. Solving this equation in the frequency domain gives:

$$\boldsymbol{x}(\omega) = \frac{e}{m(\omega_{mol}^2 - \omega^2 - i\omega\Gamma_{mol})}\boldsymbol{E}(\omega), \tag{15}$$

where $\omega_{mol}^2 = K/m$ and is called the molecular resonance frequency. Again, the optical properties come from the relationship between the polarization $\boldsymbol{P}$ and the electric field $\boldsymbol{E}$.

$$\boldsymbol{P}(\omega) = N\boldsymbol{\mu}(\omega) = N(-e)\boldsymbol{x}(\omega) = \epsilon_0\chi_e(\omega)\boldsymbol{E}(\omega). \tag{16}$$

Rearranging for χ_e and knowing that $\epsilon = 1 + \chi_e$ gives the expression for the permittivity.

$$\epsilon(\omega) = 1 + \frac{\omega_p^2}{\omega_{mol}^2 - \omega^2 - i\omega\Gamma_{mol}}. \tag{17}$$

ω_p^2 has the same definition as for metals, $Ne^2/\epsilon_0 m$ and is a material constant. This model is not completely satisfactory. Γ_{mol} is the decay rate of the emitter. It included both radiative and non-radiative decay. For optical properties, only the radiative decay is of interest. The expression for ϵ can be modified by including the oscillator strength f_1 [21].

$$\epsilon(\omega) = 1 + f_1\frac{\omega_p^2}{\omega_{mol}^2 - \omega^2 - i\omega\Gamma_{mol}}. \tag{18}$$

The dimensionless quantity f_1 is the ratio of radiative emission rate to non-radiative decay rate.

The molecules that will be used in the experiments are called Rhodamine 800 (Exciton CAS number 101027-54-7), noted as LD800. LD800 is part of the synthetic xantheno dyes [33]. Apart from the permittivity ϵ, the dipole moment μ is an important property of the molecules. LD800 has a dipole moment $\boldsymbol{\mu}$ of 4 D or 13.34×10^{-30} C m with a diameter of 1 nm [34]. Another important property of LD800 is that it agglomerates, and not aggregates. Therefore, single molecules and agglomerates have the same resonance frequency.

LD800 and by extension all Rhodamine dyes are used for many different bioanalytical methods such as fluorescence-based DNA analysis (polymerase chain reaction (PCR), quantitative PCR and gel electrophoresis) and microscopic techniques for cell analysis because of its high fluoresence quantum yields [33]. It can also be used a gain medium in a dye laser [35].

2.3 Interaction between molecules and plasmons

A molecule interacts with an electric field through its dipole moment. The interaction Hamiltonian is dependent on its transition dipole moment $\boldsymbol{\mu}$, the field intensity and their relative orientation. This interaction Hamiltonian is noted as H'. The stronger the interaction is, the higher the probability for a molecule to absorb a photon from the field or to emit a photon through stimulated emission. Fermi's golden rule says that this transition probability per unit of time, also called the emission rate, from the initial state $|i\rangle$ to a final states $|f\rangle$ is given by [1]

$$\Gamma_{i->f} = \frac{2\pi}{\hbar} |\langle i| H' |f\rangle|^2 \rho(E_f). \tag{19}$$

Note that this is the same parameter as used in Equation 14. $\langle i| H' |f\rangle$ is the matrixelement of the interaction, a factor that depends on the field intensity and the wavefunctions of the molecule. These wavefunctions are an intrinsic property of the molecule and can not be changed. On the other hand, $\rho(E_f)$ is the local density of states (LDOS) of the final level. This factor can be modified by external structures, for example by placing the molecule in a cavity. If the emitted photons can interfere constructively, the LDOS is increased, leading to a higher emission rate. When the interference is destructive, photons can not survive and the LDOS is decreased, resulting in a suppression of the emission [2].

A dielectric Fabry-Perot cavity where photons are reflected at 2 mirrors can be used to alter the LDOS, but they have their limitations. These systems are diffraction limited, meaning the volume of the modes that can exist in the cavity can not be smaller than $(\lambda/2n)^3$. λ is the wavelength of the mode, n the refractive index of the medium between the mirrors [36]. Minimizing this volume leads to an increase in the field intensity and a strong increase of the LDOS. In this thesis, a plasmonic nanoantenna will be used as a cavity. The light emitted by the molecule can be absorbed and excite plasmons in the nanoantenna in an efficient way, leading to an increased LDOS. As mentioned before, the LSP's emit light very strongly at particular places, called hotspots. Combining 2 nanorods creates a hotspot with a higher intensity. If molecules can be placed in that hotspot and the dipole moment of the molecule is aligned with the electric field of the mode, the coupling can become strong, over

10^5 times stronger than for dielectric structures [2].

The most important factor to describe the coupling is called the coupling strength g, also called coupling factor, and is defined as:

$$g = \sqrt{N}\boldsymbol{\mu} \cdot \boldsymbol{E}. \tag{20}$$

N is the amount of molecules that couple with the nanocavity and $\boldsymbol{\mu}$ the transition dipole moment. $\boldsymbol{E}$ can be rewritten is function of photon energy $\hbar\omega_{pl}$, mode volume V_m and the angle between dipole moment and electric field θ [2].

$$g = \sqrt{N}\mu\sqrt{\frac{\hbar\omega_{pl}}{2\epsilon_0\epsilon V_m}}\cos(\theta) \tag{21}$$

with $\mu = |\boldsymbol{\mu}|$. g is proportional to the interaction energy of the molecule with the field. g can be interpreted as the rate of energy exchange between molecule and cavity, but this is only true when ω_{pl} perfectly matches ω_{mol}. The value of g, compared with the plasmonic losses β_{pl} and the decay rate of the molecule Γ_{mol} will determine the properties of the coupled system. 2 regimes are distinguished: weak coupling and strong coupling. Both regimes have different properties that will be discussed. In the weak coupling regime, the LDOS of the molecule will be changed, such as to increase or decrease the emission rate. In a strongly coupled system, the molecules and cavity become one single system, with properties remarkably different from the isolated systems.

2.3.1 Weak coupling

As the name suggest, the weak coupling regime is characterized by a small value for the coupling strength g. Concretely, weak coupling is established when $g < (\beta_{pl} + \Gamma_{mol})/4$, although different definitions exist in literature, see Section 2.3.2. The macroscopic damping parameter β_{pl} can be interpreted as the cavity loss rate, while Γ_{mol} represents the molecular losses. The definition for weak coupling means that the cavity or molecular losses are higher than the energy exchange between molecule and cavity. Sometimes in literature, this regime is called bad-cavity regime, since the system has high losses [2].

If the nanoantennas are tuned to the resonance frequency of the molecules, the LDOS will be increased since the emitted photons will efficiently be absorbed by the LSP's. The factor by which the LDOS and decay rate Γ_{mol} are increased compared to free space is called the Purcell factor [37], given by

$$F_P = \frac{6\pi c^3}{n_R^3\omega_{pl}^3}\frac{Q}{V_m}, \tag{22}$$

with n_R the real part of the refractive index of the cavity, Q the quality factor of the cavity and V_m the volume of the mode supported by the cavity. The quality factor of a cavity is defined as ω_{pl}/β_{pl}. Generally, plasmonic structure have high losses, several orders of magnitude higher than dielectric structures [2]. This is compensated by the mode volume, which can be a lot smaller so plasmonic cavities can still have a higher F_P than dielectric cavities. Especially when $g > \Gamma_{mol}$, the spontaneous emission rate can be severely enhanced

[38]. Because of the enhanced emission rate and relatively high losses of the cavity, energy exchange will happen from the molecule to the cavity, but not in the reversed way since the cavity loses the photons. Therefore, a weakly coupled system has applications in fast single photon sources with a single molecule coupling to a cavity [39].

2.3.2 Strong coupling

On the other hand, for high values of g, strong coupling is established. A more precise definition for strong coupling is [40]

$$g > \sqrt{\frac{\beta_{pl}^2 + \Gamma_{mol}^2}{8}}. \tag{23}$$

This can be interpreted as a coupling strength that is high enough to overcome the losses of the emitter and cavity, and energy exchange can therefore be back and forth between the 2 components of the system. When this happens, a new single quantum system is created that is part light, part matter. Describing the system through the plasmonic properties and molecular properties does no longer suffice, even thought the new properties are largely determined by the properties of the sole components.

A nanoantenna alone has a resonance frequency of ω_{pl}, while the molecules have a resonance frequency of ω_{mol}. Both systems can be treated as oscillators, and a semiclassical model can predict what the eigenfrequencies of the coupled system are. Quantum fluctuations are neglected and it is assumed that $\omega_{pl} >> \Gamma_{mol}, \beta_{pl}$, which is valid (see Section 3). The eigenfrequencies of the coupled system are [8]:

$$\omega_{\pm} = \frac{\omega_{pl} + \omega_{mol}}{2} - i\frac{\beta_{pl} + \Gamma_{mol}}{4} \pm \Omega. \tag{24}$$

Note that here, ω_{pl} is the resonance energy of the antenna surrounded by molecules. ω_+ is called the upper polariton, while ω_- is called the lower polariton. The exact same eigenfrequencies are found with the Jaynes-Cunnings model, a simplified but full quantum mechanical model [41]. The derivation of these eigenfrequencies only considers the ideal case where the dipole moment of the molecules is parallel to the electric field. Variations of this ideal model are to be expected, with lower coupling strengths. The formation of the 2 new energy levels is somewhat different from the mode hybridization in Section 2.1.2. The charge configuration in the nanoantenna is bonding in both the polaritons and the occupation of the 2 levels differs significantly, depending on ω_{pl}, unlike the antibonding mode which is negligible. The complex frequencies $\omega_{\pm}$ can be interpreted as the frequency of a damped mode. The oscillation frequency, or the real part of $\omega_{\pm}$, is the average of the resonance frequency of the 2 components in the system, while the imaginary part is half the average of the separate damping parameters. Ω is the so-called Rabi frequency. If it is non-zero, it causes a system to have 2 different resonance peaks, both separated by the same amount from a central frequency. This phenomenon is called Rabi splitting. Figure 4 shows a schematic representation of the Rabi splitting where the LSPR matches the molecular resonance frequency. The red dot represents the molecules. The magnitude of the splitting, the vacuum Rabi frequency is

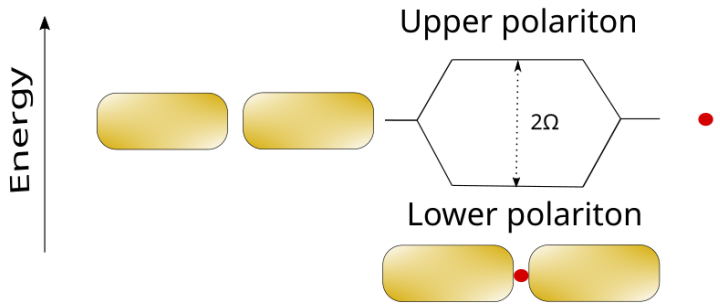

Figure 4: Rabi splitting of strong coupling between a dimer antenna and molecules

defined as

$$\Omega = \sqrt{g^2 + \frac{1}{4}(\omega_{pl} - \omega_{mol})^2 - \frac{1}{16}(\beta_{pl} - \Gamma_{mol})^2}. \tag{25}$$

The Rabi frequency defines the frequency at which there is coherent energy exchange between the plasmons and the molecules [42].

Sometimes in literature the equation for Ω is simplified by ignoring the last term under the square root to [43]

$$\Omega = \sqrt{g^2 + \frac{1}{4}(\omega_{pl} - \omega_{mol})^2}. \tag{26}$$

As mentioned before, g can be interpreted as the energy exchange rate, but this in only true when ω_{pl} matches ω_{mol}. This can be seen from Equation 26, since $\Omega = g$ in that case. In order to have a real splitting in the resonance frequencies of the system, Ω has to be real and in order to have 2 clear peaks, the splitting has to be bigger than the linewidth of the unsplit spectrum. β_{pl} and Γ_{mol} are defined as the linewidths of the emission spectra of the plasmons and the molecule respectively, but the linewidth of the coupled system is $(\beta_{pl} + \Gamma_{mol})/4$. Assuming that $\omega_{pl} \approx \omega_{mol}$, which is the case if the LSPR is tuned to the molecular resonance frequency, the condition for strong coupling becomes

$$\sqrt{g^2 - \frac{1}{16}(\beta_{pl} - \Gamma_{mol})^2} > \frac{\beta_{pl} + \Gamma_{mol}}{4}. \tag{27}$$

Solving for g gives Equation 23. If the term $(\omega_{pl} - \omega_{mol})$ cannot be ignored, the coupling strength g will be smaller for a given Ω, making strong coupling more difficult. It has to be noted that sometimes in literature, another definition for strong coupling is used [2, 5]:

$$g > \beta_{pl}, \Gamma_{mol}, \tag{28}$$

and sometimes

$$g > \frac{\beta_{pl} + \Gamma_{mol}}{4}. \tag{29}$$

This last definition results in a positive value under the square root in Equation 25, but does not consider the linewidth of the emission spectra. Nevertheless, 2 peaks are visible in

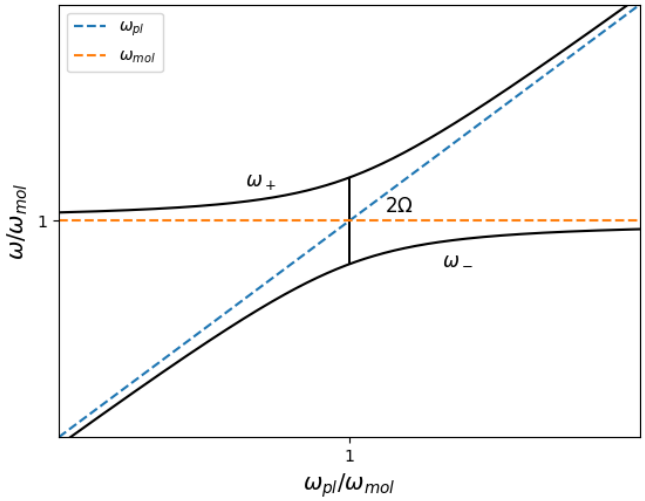

Figure 5: Anticrossing behaviour of a strongly coupled system

the scattering spectrum if this condition is satisfied. This definition will be used in this thesis.

Another property of strongly coupled systems is anticrossing. This means that the eigenfrequencies of the system, the upper and lower polariton $\omega_{\pm}$ should not cross each other if the plasmonic resonance frequency is changed. Figure 5 shows this behaviour. The point where the 2 dotted lines cross is where the plasmonic resonance frequency matches the molecular resonance frequency, $\omega_{pl} = \omega_{mol}$. If the coupling strength g is high enough, strong coupled is reached and the 2 polaritons are separated by a distance 2Ω. If ω_{pl} is then changed, by changing the length of the nanoantenna for example, the 2 polaritons approach the resonance frequencies of the sole nanoantenna and the sole molecules without crossing each other [44].

The applications for strongly coupled systems vary widely. Single-atom lasers can be made, as well as ultralow-threshold lasers [45, 46]. The efficiency of non-linear processes can be boosted severely by matching the harmonics to the cavity [47]. Another application is efficient light harvesting. By creating a strongly coupled system between Au nanoparticles and TiO_2 molecules that matches a part of the spectrum of sunlight, the absorption of light is enhanced. The nanoantenna is connected to a circuit where the electrons from the plasmonic oscillations can flow to. The circuit can then capture the energy of the generated current [12, 13]. However, the most promising applications lie in quantum information for the creation and preservation of a qubit that is part light, part matter through a strongly coupled system [11, 48].

3 Numerical simulations

To verify the theory described before and calculate exact values for ω_{pl}, β_{pl} and Ω, finite difference time domain (FDTD) simulations were carried out using the commercial software Lumerical. In this thesis, both rod and dimer nanoantennas are investigated and the interest is solely in the far field and scattered field of the nanoantennas. Since ω_{pl}, β_{pl} and Ω are visible in the scattered field, only the scattered field data will be shown. In all the simulations, the dimers are symmetrical, meaning they consist out of 2 identical rods. The layout of the simulations is made as realistic as possible. It includes the glass substrate the nanoantennas are attached to and a layer of indium tin oxide (ITO) of 9 nm thickness, see Section 4.1. As mentioned before, the nanoantennas and their optical properties are completely determined by their length, gap, radius of curvature on the edges and material constants. The nanoantennas are made out of Au, with the optical properties measured by Johnsen and Christy [17] since these values correspond best with the measurements. The measured values are imported into Lumerical. These values are shown in Figure 6, where Figure 6a and 6b show the real and imaginary part of the permittivity ϵ respectively. A trendline is then fitted and shown in blue. Since the material for the nanoantennas is not changed, the only tunable factors are the geometrical ones. More so, only the length and gap are varied. The width and the height of the rod is chosen as 50 nm and the radius of curvature 10 nm.

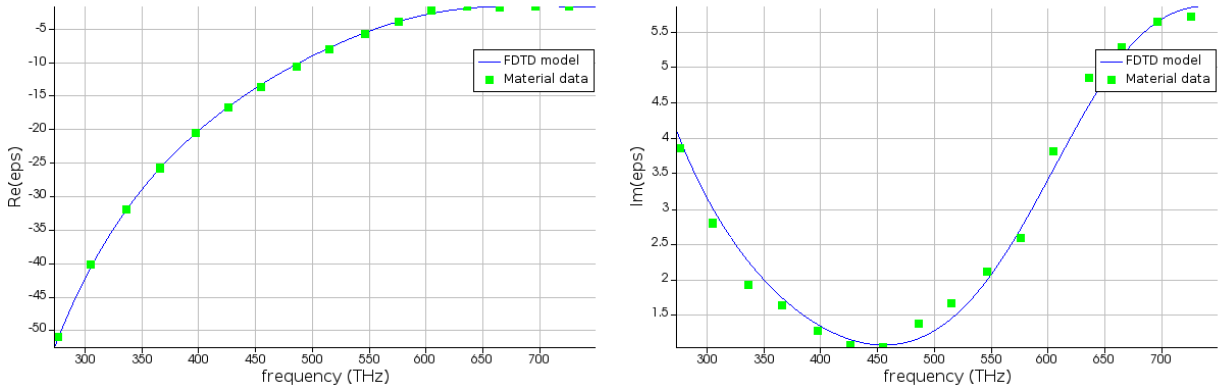

(a) Real part of the permittivity

(b) Imaginary part of the permittivity

Figure 6: Permittivity of Au

3.1 Nanoantennas

First, simulations are carried out with nanoantennas without molecules. This way, insight is gained on how the frequency of resonance can be tuned by varying the length and gap size of the nanoantennas. The layout for the simulations is shown in Figure 7, in this case a nanoantenna with length 60 nm and gap 5 nm. The red material is the glass substrate. The brown material is the ITO layer. The 2 yellow structures are the nanorods. The grey box surrounding the nanoantenna is the source. Here, a total field scattered field (TFSF) source was chosen. As the name suggests, both the total field and the scattered field can

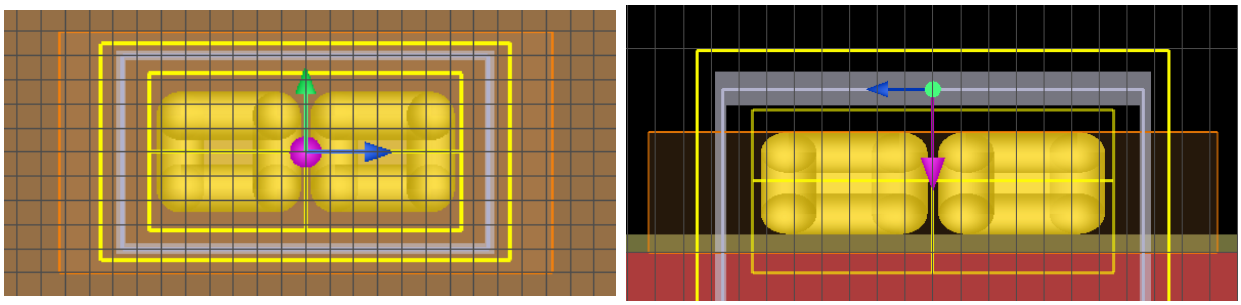

(a) Top view of the nanoantenna

(b) Side view of the nanoantenna

Figure 7: Layout of the nanoantenna simulations

easily be measured with this source. Inside the box, the total field is simulated and outside the box only the scattered field. This means that only the scattered field is present outside the box, the reflected field is subtracted from the outgoing wave. The pink arrow indicates the direction of propagation of the source. This is different from the way the measurement setup is built, see Section 4.2. However, the goal from the simulations is to get the resonance frequency ω_{pl} and FWHM of the scattering cross section β_{pl} and this remains the same for the measuring methods. The blue arrow is the polarization of the electric field, the green one of the magnetic field. The polarization of the source makes a big difference in resonance frequency, see Equation 12. In all simulations and measurements, the electric field is parallel to the long side of the nanoantenna. Then, there are 2 yellow boxes surrounding the nanoantenna. The inner one monitors the total near field and as mentioned before, this data is not of interest in this thesis. The outer one monitors the scattered field.

The obtained data from the simulations is displayed as a scattering cross section σ_{scat}. The scattering cross section is defined as the total power scattered in all directions divided by the incident power flux [25] and is normalized for the spectrum of the source.

Figure 8 shows cross sections for 4 different lengths, $L = 60$, 90, 120 and 150 nm and for different gaps, ranging from 5 to 30 nm. The results for rod antennas are also shown. The lower limit on the y-axis is 0 in every plot, the upper value is different for every plot. A first observation is that the scattering cross sections have a Lorentzian shape. It can be seen that for smaller gaps, the peak of the scattering cross sections is higher, meaning the scattering happens more efficiently compared to nanoantennas with larger gaps. For rod antennas, the peak is remarkably lower. Figure 9 compares the scattering cross sections for nanoantennas with a gap of 20 nm with different lengths. It is clear from the Figure that longer nanoantennas have a higher amplitude in their scattering cross sections. This is solely a consequence from the fact that longer nanoantennas have a bigger surface to scatter from. This also explains why a rod has a lower scattering amplitude, it only has half the surface of a dimer. The resonance frequency, ω_{pl} is defined as the frequency of the peak in the scattering cross section. In Figure 10a, the resonance frequencies are plotted for all the dimer simulations. This resonance frequency corresponds to the bonding mode in the dimers. The antibonding mode is not visible is the scattering cross section. A couple of clear observations that hold

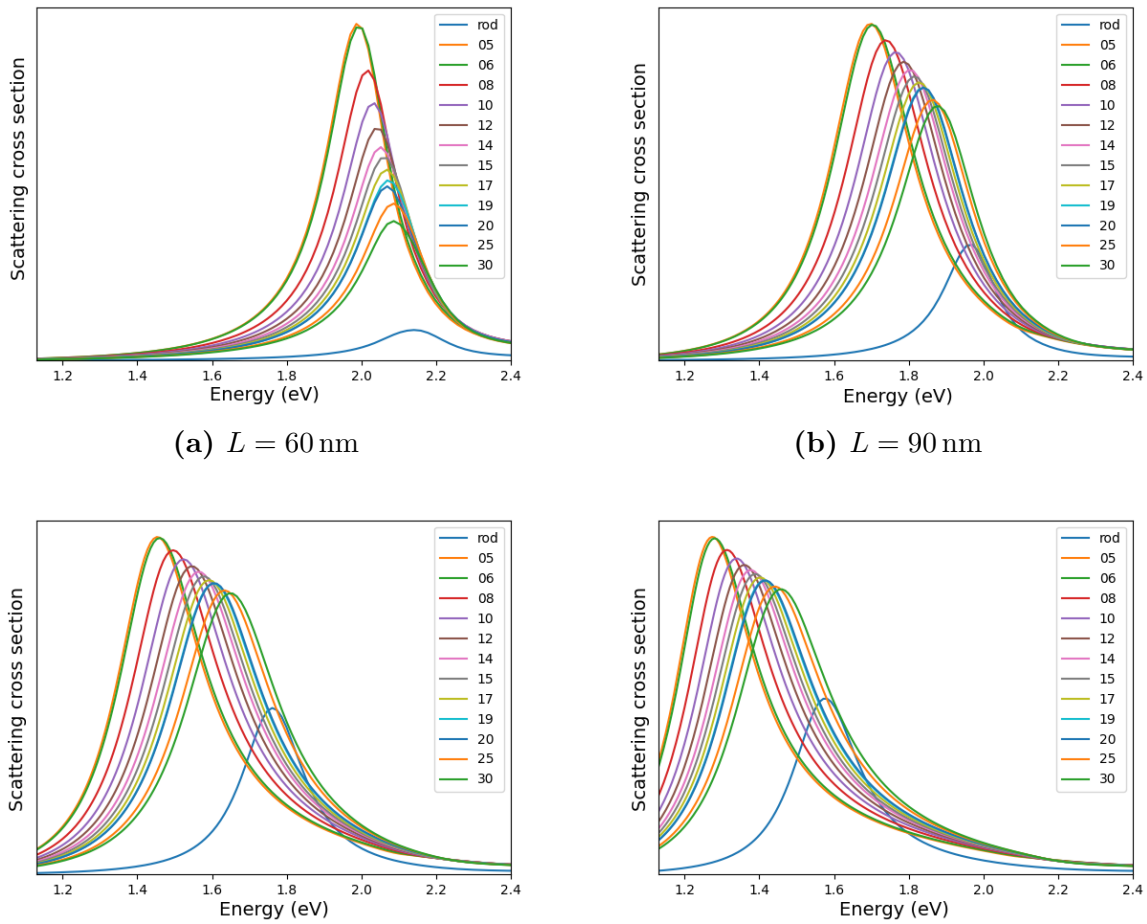

(a) $L = 60\,\text{nm}$ **(b)** $L = 90\,\text{nm}$

(c) $L = 120\,\text{nm}$ **(d)** $L = 150\,\text{nm}$

Figure 8: Scattering cross sections for different dimers

for every nanoantenna can be made from this Figure.

First, the resonance energy is higher for smaller nanoantennas. This is in agreement with the theoretical model. From Equation 12, it is known that smaller nanoantennas correspond with higher resonance frequencies. Secondly, the resonance frequency is higher for bigger gaps. This is also expected from the theoretical model since a smaller gap increases the hybridization of modes. The resonance frequency of a dimer approaches the resonance frequency of a rod for an increasing gap size.

The macroscopic damping of the plasmonic oscillations in a nanoantenna is described by the parameter β_{pl}, see Equation 13. As mentioned before, β_{pl} is the FWHM of the scattering cross section. Figure 10b shows β_{pl} for every simulation. This parameter is a property of the sole nanoantenna and not the system with molecules, but is an important aspect in the distinction between the weak and strong coupling regime. Therefore, it is important to know β_{pl} for every nanoantenna. 2 similar observations can be made from Figure 10b. β_{pl}

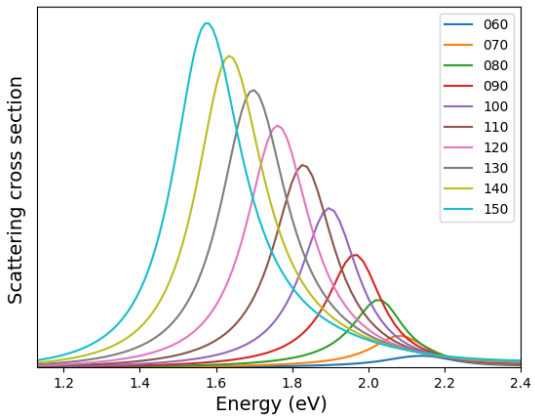

Figure 9: Comparison between scattering cross sections of nanoantennas with different lengths and a gap of 20 nm

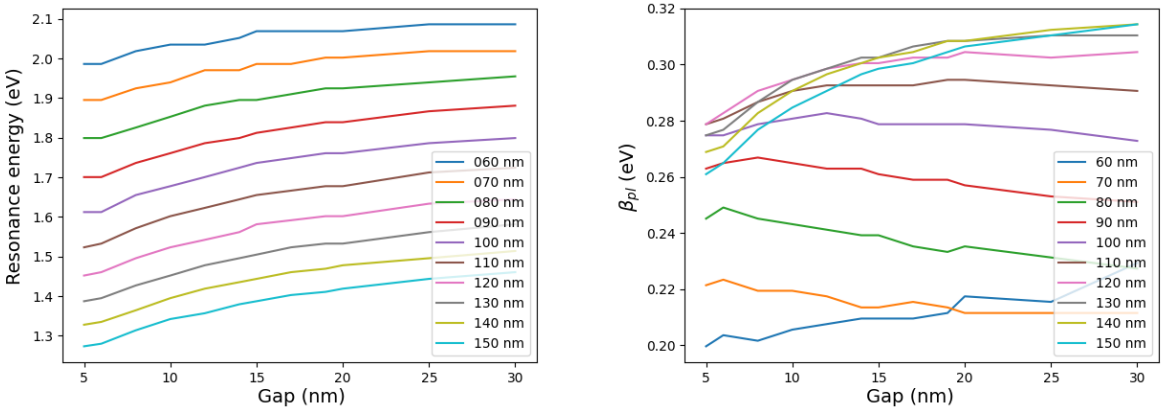

(a) Resonance energy ω_{pl} **(b)** β_{pl}

Figure 10: Resonance energy and damping β_{pl} for all the simulated dimers

decreases for smaller lengths and increases for higher gaps. It has to be mentioned that the change with different lengths is more pronounced than with gap sizes. For all the simulated lengths, β_{pl} is smaller for rods than for dimers.

In the fabrication of nanoantennas (see Section 4.1), there will always be variations in the radius of curvature. For completeness, Figure 11 shows the scattering cross section for 3 dimer antennas with length 70 nm and gap 20 nm and with radii of curvature of 5, 10 and 15 nm. The resonance frequency ω_{pl} for the 3 nanoantennas are 1.94 eV, 2.00 eV and 2.07 eV respectively, while the values for β_{pl} are 0.202 eV, 0.210 eV and 0.218 eV respectively. This can be generalized, a higher radius of curvature leads to a higher resonance frequency ω_{pl}, to a higher linewidth β_{pl} and also to a lower intensity of the scattered field.

In Section 2.1.2, it has been mentioned that the reason dimer antennas are preferred over

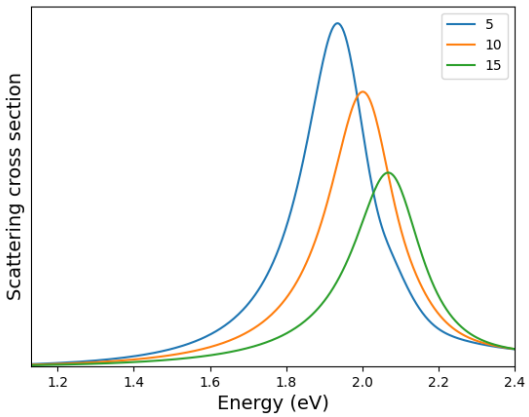

Figure 11: Scattering cross sections for dimers with length 70 nm and gap 20 nm with different radii of curvature

rod antennas is that the field intensity in their hotspot, the gap, is higher than in the hotspot of a rod and that the smaller the gap is, the higher the intensity. Figure 12 compares the optical power of the resonance frequency of a dimer with a small gap, a dimer with a big gap and a rod. The plane that is shown is parallel to the substrate, through the middle of the nanoantennas, i.e. 25 nm above the ITO layer. As said in the theory, the hotspot of a dimer is in the gap, while the hotspot of a rod in at the edges and along the short side of the rod. That is now confirmed through the simulations. It can clearly be seen that the optical power is highest in the dimer with the smallest gap, followed by the dimer with the wide gap and by the rod. It has to be mentioned that a dimer with a gap of 30 nm only gives a small field enhancement. Another observation is that the power inside of the nanoantennas is very small. This is in agreement with the theory, saying that light cannot propagate large distances inside Au. The gaps in Figure 12a and 12b are 5 and 30 nm respectively. The mode volume V_m of the emitted light can be approximated by the volume of the gap [49], here $50\,\text{nm} \times 50\,\text{nm} \times 5\,\text{nm}$ and $50\,\text{nm} \times 50\,\text{nm} \times 30\,\text{nm}$ or $12\,500\,\text{nm}^3$ and $75\,000\,\text{nm}^3$ respectively. This is well beyond the diffraction limit of conventional dielectric cavities [2], where the minimal mode volume is $(\lambda/2n)^3$ [50]. This corresponding to roughly $40\,000\,000\,\text{nm}^3$ in air for $\lambda = 682\,\text{nm}$. Estimating the mode volume for a rod as in Figure 12c is harder, since the mode is not confined and stretches out. For this reason, it can be said with certainty that the mode volume will be higher [2].

Finally, to demonstrate the dependence on the polarization known from Equation 12, Figure 13 shows the scattering cross sections for dimers with lengths from 60 nm to 150 nm and a gap of 20 nm and for a rod of 50 nm. In the simulations, the polarization of the source is set to be perpendicular to the long side of the nanoantennas, thus to excite the dipole along the short side of 50 nm. As mentioned before, the length of the nanoantenna and the gap have no influence on the resonance frequency. ω_{pl} only shifts from 2.20 eV to 2.22 eV over the whole length range and matches the 50 nm rod perfectly.

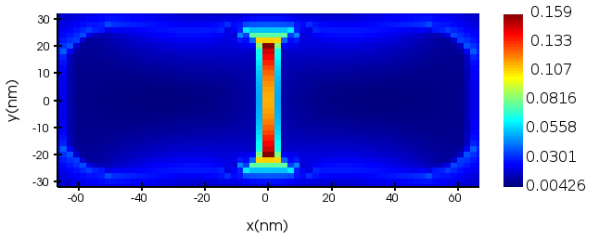

(a) Dimer with length 60 nm and gap 5 nm

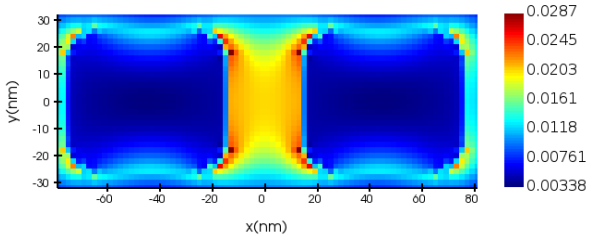

(b) Dimer with length 60 nm and gap 30 nm

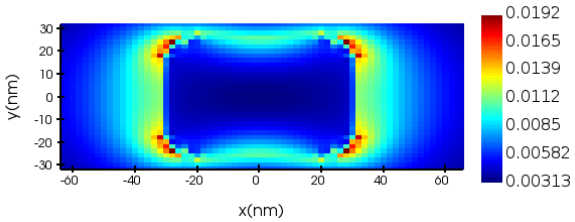

(c) Rod with length 60 nm

Figure 12: Cross section of the optical power (in Watt) of the resonance frequency of the nanoantenna in a plane parallel to the substrate

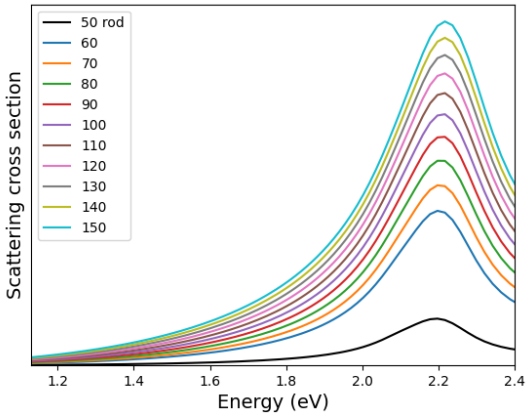

Figure 13: Scattering cross sections for dimers with different lengths and a rod with the polarization of the source perpendicular to the nanoantenna

From this section, a clear idea can be obtained of which nanoantennas are suitable for obtaining strong coupling with LD800 molecules. On the one hand, the nanoantenna needs to have its resonance frequency ω_{pl} as close as possible to the molecular resonance frequency ω_{mol}. Figure 10a gives a clear overview of which nanoantennas comply. On the other hand, the nanoantenna needs to have a small β_{pl}. This way it is easier to accomplish strong coupling, see Equation 29. This corresponds with long nanoantennas and to a lesser extent to nanoantennas with a high gap size. It is also desirable to have a field intensity as high as possible at the hotspots of the nanoantenna. Since the coupling strength g is proportional to the field amplitude, or alternatively inversely proportional to the square root of the mode volume, see Equation 20 and 21, a small gap size is desirable. This is confirmed by Figure 12. The mode volume is after all proportional to the gap size.

3.2 Nanoantennas and molecules

The layout for the simulations of nanoantennas with molecules is very similar as in the previous section. Only the molecules have to be added, as is shown in Figure 14, where the upper red layer represents the molecules. For the simulations to be similar to the experiments, the layer has a thickness of 20 nm. In the simulations, the dipole moments of the LD800 molecules is not included. Therefore, variations from Equation 24 are expected. Note that in the area where the nanoantennas and the layer of molecules overlap, the material constants for the nanoantenna are used in the simulations.

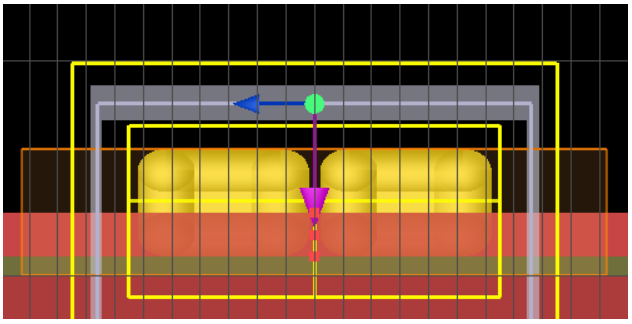

Figure 14: Layout of the nanoantenna with molecules simulations

The optical properties of LD800 are retrieved from measurements. Fitting Equation 18 to experimental data gives the data for the permittivity of LD800 shown in Figure 15 (see Section 5.1). Figure 15a and 15b show the real and imaginary part of the permittivity ϵ respectively. The peak in the imaginary part ω_{mol} is at 440 nm, corresponding to an energy of 1.82 eV. The linewidth Γ_{mol} of the peak in the imaginary part corresponds to 0.116 eV.

The results for the simulations of nanoantennas with 4 different lengths, 60, 90, 120 and 150 nm are plotted in Figure 16 in the form of scattering cross sections. The gaps range from 5 to 30 nm and also single rods are included. Note that the y-axis starts at 0 for every plot but is different for different plots. As described in Section 2.3.2, a strongly coupled system

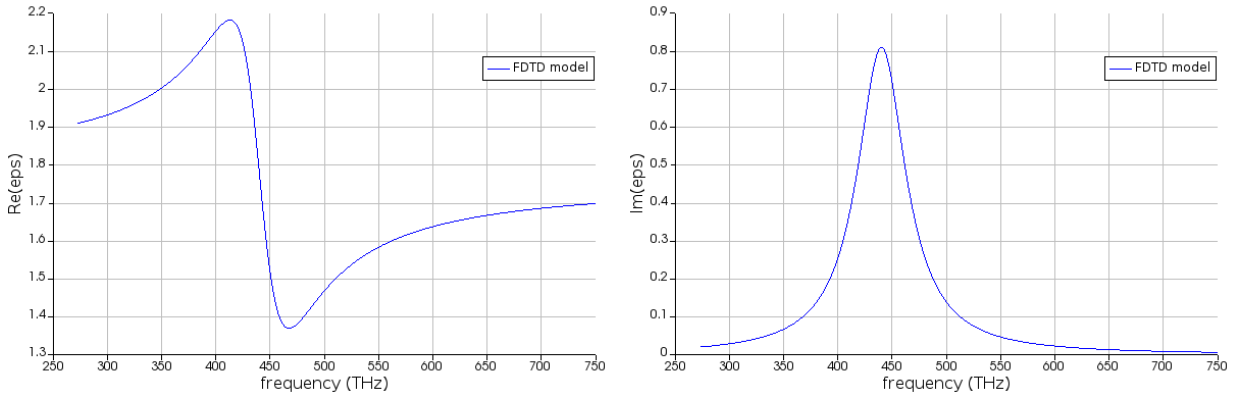

(a) Real part of the permittivity **(b)** Imaginary part of the permittivity

Figure 15: Permittivity of LD800

exhibits 2 peaks, separated by twice the Rabi frequency, 2Ω. The peak with the highest frequency is called the upper polariton, the peak with the lowest the lower polariton. In Figure 16a and 16b, all the nanoantennas exhibits 2 maxima and are therefore strongly coupled. Also nanoantennas with lengths 70, 80 and 100 nm show strong coupling. Figure 16c and 16d show no strong coupling, the same holds for nanoantennas with 110, 130 and 140 nm lengths.

A couple of observations can be drawn from the simulations. The dip between the 2 peaks is at the resonance frequency of the molecules, 1.82 eV. Less light is scattered at the frequency because it is absorbed by the layer of molecules. This dip is not in the middle of the 2 peaks and is therefore not the central frequency. The central frequency is defined as $(\omega_{pl} + \omega_{mol})/2$. ω_{pl} for a nanoantenna surrounded by air is known from the simulations of nanoantennas only and shown in Figure 10a. From Equation 12, it is known that a natural decrease of ω_{pl} will occur due to the presence of the molecule, even when they don't couple to each other. The central frequency in the simulations shifts with $0.051 \pm 0.006\,\text{eV}$ from the expected value. Therefore, the presence of this particular amount of molecules decreases ω_{pl} with $0.102\,\text{eV}$ on average. It is known that ω_{pl} increases with increasing gap size and with decreasing length, the central frequency follows the same trend. Another observation is that the amplitude of the scattering cross sections increases with decreasing gap size and with increasing length, as is the case for sole nanoantennas. The effect of increasing length is shown on Figure 17. Also remarkable is the relative amplitude of the 2 peaks. When ω_{pl} is higher than ω_{mol}, the upper polariton has a higher peak than the lower polariton and vice versa.

Figure 18 shows Ω for the simulations where strong coupling is established and from Ω and the knowledge of $\omega_{pl}, \beta_{pl}, \omega_{mol}$ and Γ_{mol}, the coupling strength g is calculated using Equation 25. The shift of ω_{pl} due to the presence of the molecules is taken into account for the calculation of g. In Figure 18b, the lines are the calculated coupling strengths g and the dots are the minimal values for strong coupling, $(\beta_{pl} + \Gamma_{mol})/4$ as said in Equation 29. This confirms the theoretical model for the minimal value of g. This knowledge is important for the experimental measurements. If 2 peaks appear in the scattering spectra

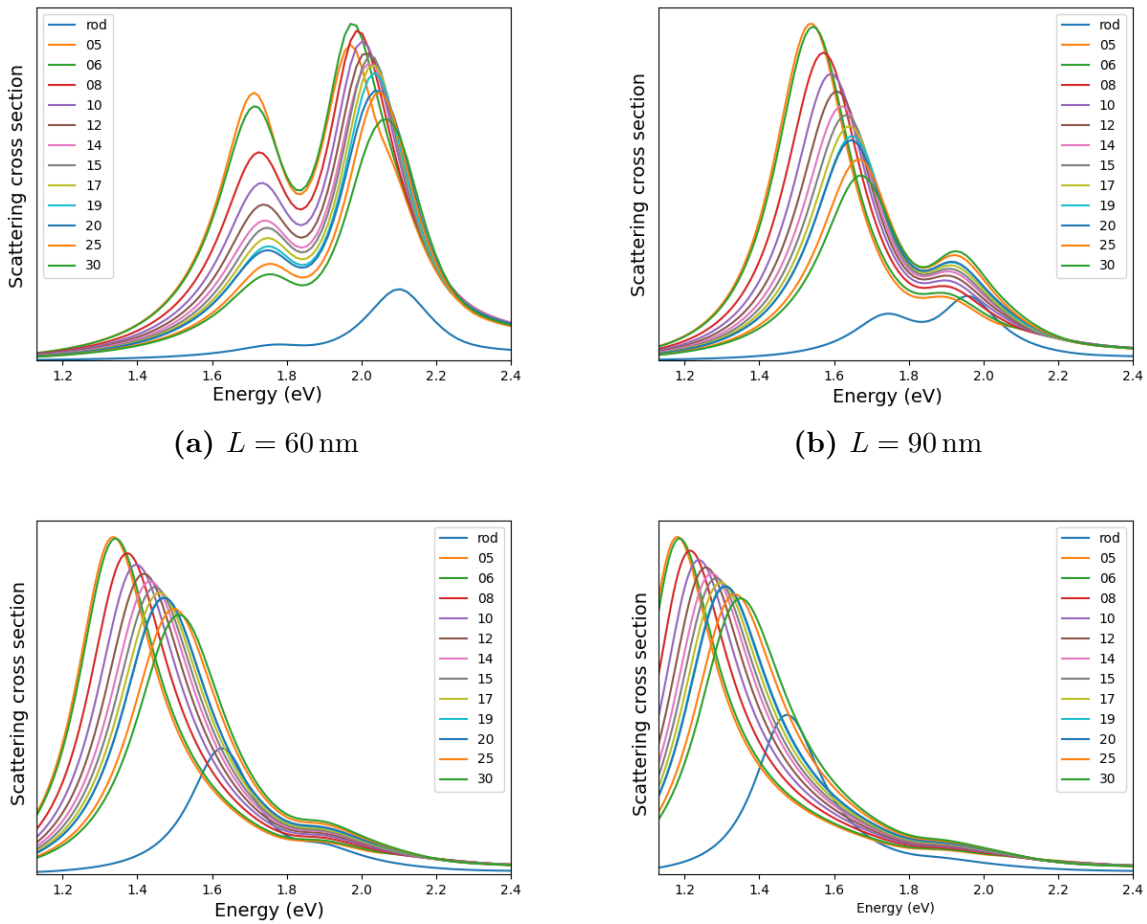

(a) $L = 60\,\text{nm}$ **(b)** $L = 90\,\text{nm}$

(c) $L = 120\,\text{nm}$ **(d)** $L = 150\,\text{nm}$

Figure 16: Scattering cross sections for different dimers with molecules

of the nanoantennas with molecules, strong coupling is indeed established. The observations from Figure 18b match the theoretical predictions. Smaller gaps correspond with a higher value of g due to their strong field intensity. Another observation is that longer dimers have a higher coupling strength. In Figure 10a, all the resonance frequencies are shown. It can be seen that nanoantennas with length 60 and 70 nm have a resonance frequency well above the molecular resonance frequency, while the nanoantennas with length 80, 90 and 100 nm correspond better.

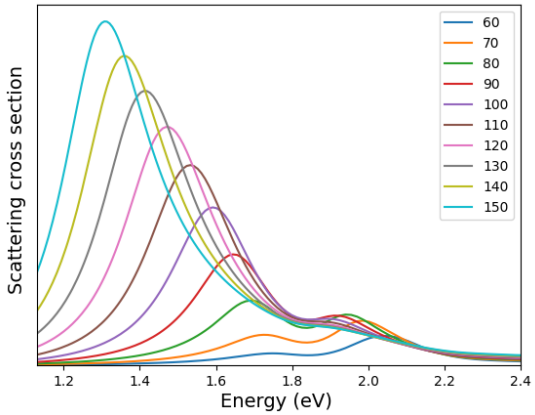

Figure 17: Comparison between scattering cross sections of nanoantennas with molecules with different lengths and a gap of 20 nm

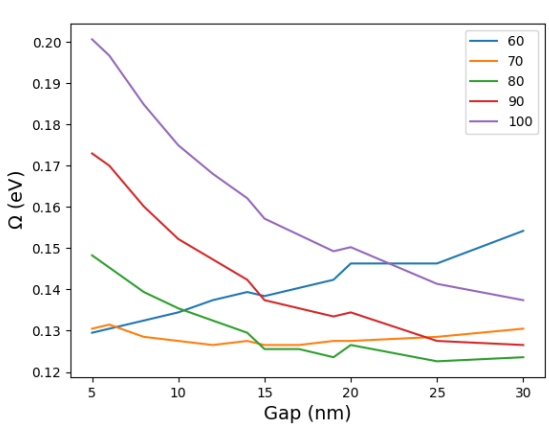

(a) Rabi frequency Ω

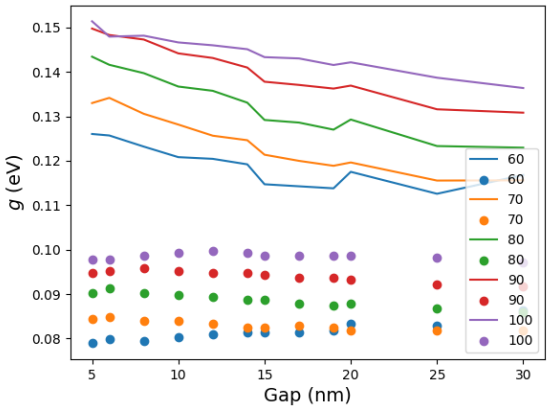

(b) The lines represent the calculated value for g, the dots the minimal value for strong coupling

Figure 18: Observed Ω and calculated g for the simulations where strong coupling is observed

4 Methods

In this section, the fabrication of the samples with nanoantennas will be discussed. The used technique is called electron beam lithography. Then, the experimental setup to measure the scattered field is given and the method of how the wanted information is obtained from the raw measurement data.

4.1 Fabrication

Electron beam lithography (EBL) is a popular technique for fabrication of nanostructures. The principle of EBL is that customs shapes can be drawn on a substrate covered with an electron-sensitive film [51]. Parts of the sample will be radiated with electrons. The parts of the film that are radiated will change their chemical structure. In the case of this thesis, they will soften and become soluble. Electrons, unlike photons, do not suffer from diffraction and therefore EBL has a smaller minimum feature size. The resolution is pushed down to 1 nm in specialized systems [52]. Here however, the controllable minimum feature size is 10 nm.

EBL requires a conductive surface to draw the desired shapes. A insulator would accumulate the charges of the electrons that are sent to the sample. Therefore, a layer of indium tin oxide (ITO) is applied. The ITO layer has a double function: it is conductive and therefore makes EBL possible, while it also increases the adhesion of Au to the glass substrate. The layer is 9 nm thick. ITO is evaporated and deposited on the glass substrate, then annealed until the sample is transparent again. An electron-sensitive layer is then added on top of the substrate and spin coated. This layer is 200 µm thick. Subsequently, the sample is annealed at 150 °C for 5 minutes. Figure 19 shows the steps of the lithographic process. In step II the electron-sensitive film (marked as 2) is applied on the substrate (marked as 1).

Once this film is present, the substrate can be mounted in the EBL equipment (Raith SEM-FEG INSPECT F50) to draw the desired shapes. The electron beam will radiate the sample where the nanoantennas will come. An important parameter is the dose of the beam. The dose is defined as the charge per unit area that is incident on the sample. Different values for the dose can change the quality of the nanoantennas severely, meaning that the value for the dose has to be optimized through a iterative process of fabricating, measuring and analysing. The optimized dose is 330 $\mu C/cm^2$.

A sample consists of so-called arrays of nanoantennas. An array is a rectangle with 9 rows and 10 columns. The length of the nanoantennas is varied in the columns from 60 to 150 nm. Accordingly, the difference in length between 2 columns is 10 nm. The width and height of an antenna are both 50 nm. All rows are intended to be identical. In the fabrication process, variations in all the dimensions will occur, see Section 5. Every sample has arrays with rods and arrays with dimers. For the arrays with dimers, the gap size is constant for individual arrays, but varies for different arrays. The spacing between adjacent rows and between adjacent columns is both 4 µm, making it possible to illuminate single nanoantennas or collect the scattered signal from single nanoantennas. Every array has a label, mentioning the dose, the range of the lengths of the nanoantennas and the gap. The spacing between

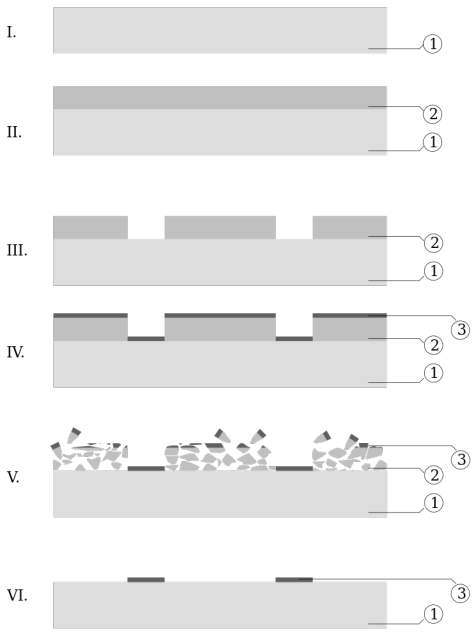

Figure 19: Schematic representation of the lithography process

different arrays is 50 µm. All the nanoantennas are drawn individually on the sample by the EBL machine.

When this process is finished, the sample is submerged in a solvent, here a mixture of 3:1 of methyl isobutyl ketone and isopropyl alcohol (MIBK:IPA). The unexposed areas are insoluble by the solvent, while the exposed areas are soluble and are removed. This corresponds to Step III in Figure 19.

The next fabrication step is the deposition of Au uniformly over the sample. The thickness of the deposited layer is 50 nm, the same as the width. Since the thickness of the electron-sensitive film is 200 µm, the deposited Au on top of the electron-sensitive film is not in contact with the deposited Au in the areas where the electron-sensitive film is removed. This makes the lift-off technique possible, see step IV in Figure 19. The deposition rate of Au is 0.1 nm/s. A different solvent is then used to remove the unexposed areas of the electron-sensitive film (Step V). Submersion is done in acetone for 3 hours at 50 °C. After dry blowing with nitrogen, the sample with sole nanoantennas is ready.

A scanning electron microscope (SEM) is used to obtain images from individual nanoantennas or from bigger parts of the sample. The SEM images are a useful tool obtain an idea of how well the nanoantennas are fabricated. Their length, gap size and radius of curvature can be measured. It can also be checked which arrays are dust free before measuring. Figure 20 shows a single nanoantenna from the sample with the optimized dose. It is clear from the Figure that the nanoantennas don't have flat sides and that the radius of curvature is different at different edges.

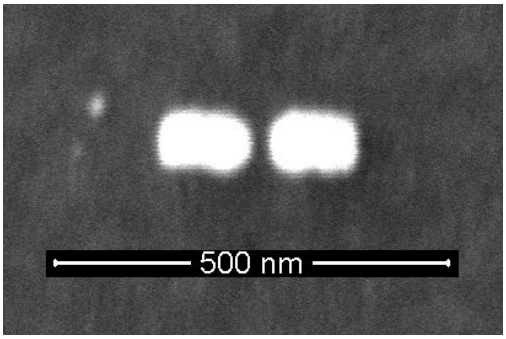

Figure 20: SEM image of a dimer nanoantenna

If the sole nanoantennas are measured and the results are desirable, LD800 molecules are added to the same sample. First, a solution of LD800 in ethanol is prepared. It is not possible to know the exact concentration, but the intention is to have a solution of 150 mM of LD800 in ethanol. The solution is added to a sample with nanoantennas and spin coated at 1000 rpm for 30 seconds. A thin layer of 20 to 25 nm of LD800 solution is then formed over the whole substrate. The molecules added to the sample evaporate over time. Therefore it is important to measure shortly after the fabrication.

4.2 Measurement setup

The method that is used in this thesis to measure the scattered field of the nanoantennas is wide-field and dark-field microscopy. The reason why wide-field microscopy is suited is because it can illuminate a complete array of nanoantennas at once and therefore a complete array can be measured at once, making the measurement a lot less time consuming compared to confocal microscopy, where every nanoantenna is measured individually. The downside of this method is that not every nanoantennas will be completely in focus and the resolution is of wide-field microscopy is lower in theory. In practice, confocal microscopy gives little resolution improvement over wide-field [53]. In dark-field microscopy, a mask is placed between the sample and the detector and the light that is reflected and scattered by the sample is focused onto that mask. The mask only blocks the reflected light since the biggest part of the scattered light has a different direction of propagation and is not in focus on the mask. Accordingly, only the scattered field reaches the detector. A dark-field microscopy setup is chosen since nanoantennas have a relatively low scattered field because of their small size and it would be challenging to distinguish the scattered field from the reflected field. With the dark-field mask, this difficulty is overcome without loss of information, since all the information of interest (ω_{pl}, β_{pl} and Ω) is visible in the scattered field. In the next paragraphs, all the parts of the setup will be discussed. Figure 21 shows a schematic representation of the complete setup. All the measurements are carried out at room temperature.

To illuminate the sample, it is desirable to have a flat spectrum over the range of interest, i.e. the range where the resonances of the nanoantennas are. If a sample is illuminated with a spectrum that is not flat, even after normalization, unexpected peaks or dips may appear

in the spectrum of the scattered field. A flat spectrum can avoid these. In practice, obtaining a perfectly flat spectrum is impossible. If the intensity variations in the flat part are less than 5%, there is no need for normalization anymore.

To achieve a flat spectrum, a pulsed laser, (SuperK Extereme EXR-20 by NKT Photonics, part 1 in Figure 21) is used with a repetition rate of 78 MHz. In order to get the spectrum flat, the spectral components of the laser beam are split by a grating (part 2). A spatial light modulator (SLM, part 3) is positioned in the Fourier plane of the grating. The SLM consist of 640 pixels of which the reflection can be controlled separately by changing the applied voltage to the pixel. This can be done for 2 polarizations independently. Since the spectral components of the laser beam are split, every pixel controls the reflection of 1 frequency. By decreasing the reflection of the frequencies where the intensity is high and vise versa, the spectrum can be made flat. The reflected light is again incident on a grating that converges the light into a single beam.

On top of the voltage mask that results in a flat spectrum, an effective phase modulation is applied to every pixel of the SLM. The following equation is employed [54].

$$I(\omega, t) = |\cos((\omega - \omega_0)t)|^2. \tag{30}$$

I is the reflected intensity, ω the frequency that is incident on the pixel of the SLM and ω_0 is the frequency of the rotating frame. This results in an effective phase modulation that is frequency dependent. By doing so, this system becomes an effective Michelson interferometer.

The next step is to reduce the speckles in the beam by decreasing the coherence of the beam. This is done in 2 steps. First, the beam is reflected by 2 galvanometer mirrors (GM, part 4 and 5). A GM is a mirror that moves back in forth in 1 direction with a certain frequency. The 2 GM's move in 2 perpendicular directions. Using an objective (Olympus, NA 0.25, magnification of 10), the beam is then coupled into a multimode fiber with a 100 µm core (part 6). The different excited modes have different propagation constants so they will move at a different speed, reducing the coherence of the beam. At the end of the fiber another objective (Olympus, NA 0.4, magnification of 20) is placed that makes sure the beam travels further without diverging. These 2 techniques together make sure there are no more speckles in the beam before illuminating the sample.

A linear polarizer (part 7) is mounted after the fiber since there is only 1 polarization of interest here, parallel to the nanoantennas. Also a neutral density (ND, part 8) filter is inserted to increase or decrease the intensity without changing the spectrum.

Subsequently, the sample is illuminated. The beam is focused by a lens (part 9) on a movable rod mirror (part 10) that reflects the light through an oil-immersion objective (Nikon lambda series, NA 1.4, magnification of 60, part 11). The sample (part 12) is mounted on the other side of the objective on a movable sample holder, so the reflected and a part of the scattered light travel through the objective again. Behind the objective, the dark-field mask

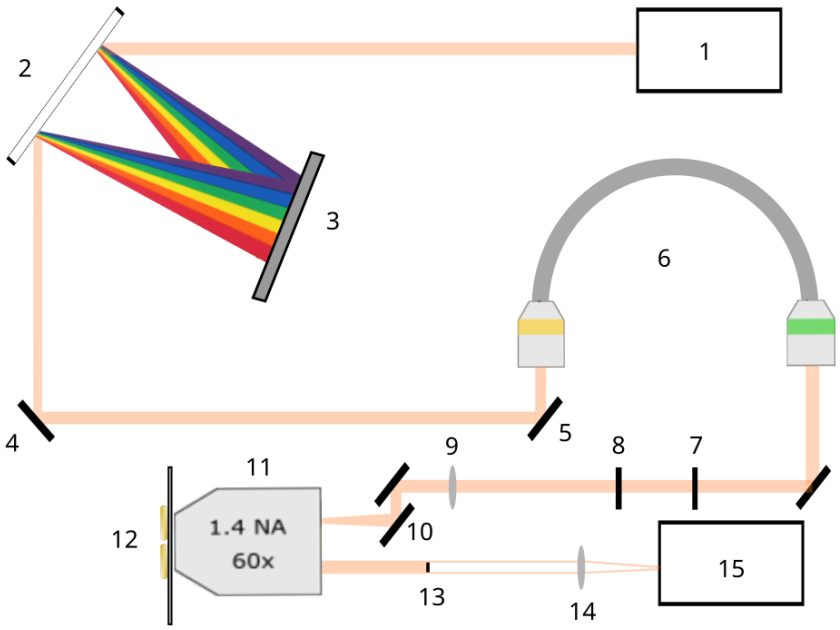

Figure 21: Schematic representation of the setup

(part 13) is mounted and only the scattered field travels past the mask onto a lens (part 14) that focuses the beam onto the detector.

The measurements are done with an EMCCD camera (ImagEM C9100-13 by Hamamatsu, part 15). The EMCCD has 512 by 512 pixels of 190 nm by 190 nm each. Figure 22 shows how a dark-field image looks like. The image from the EMCCD allows moving the sample holder to get the nanoantennas in focus. The 3 dots on the upper right, upper left and lower left are 3 reference points, below the array is the label. The nanoantennas on the right appear brighter than the ones on the left since they are bigger. The time step between measurements is 0.5 fs. By creating a feedback loop between the EMCCD and the SLM, the mask of applied voltages is created for the SLM that results in a flat spectrum. Figure 23 shows the measured laser spectrum with a glass substrate mounted in the sample holder. This graph is the average spectrum of all the pixels at the EMCCD. It can be seen on the Figure that the spectrum is approximately flat in the region between 1.5 and 2.1 eV. How broad the flat part can be depends on the maximum frequency with which the SLM can change the reflection of a pixel, as can be seen from Equation 30. A new mask for the SLM has to be created every time the laser is switched off and on, since the variations in the intrinsic laser spectrum are too high for the same mask to be used.

4.3 Data analysis

Once samples are measured, the raw data in the form of an image of 512 by 512 pixels has to be processed. Every measurement is done twice, every time accompanied with a background measurement. The background measurement includes light from ambient sources and the dark counts of the EMCCD. After the background is subtracted, an image is obtained from

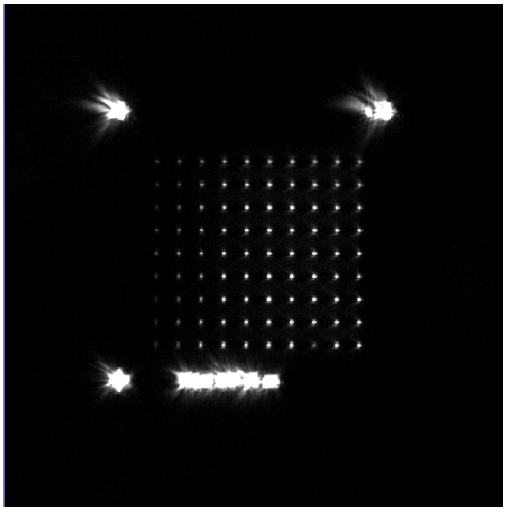

Figure 22: Image of an array of nanoantennas at the EMCCD

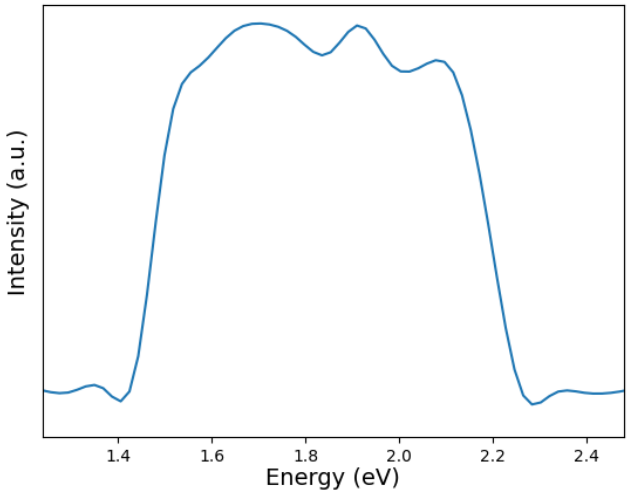

Figure 23: Laser spectrum averaged out over all the pixels at the EMCCD

a complete array of the nanoantennas and the surrounding. A rectangle containing only the scattered field of the nanoantennas is cut out of the total image and intensity peaks in the image corresponding to the nanoantennas are selected. Cutting out the rectangle is needed because as mentioned in Section 4.1, an array has a label with a big size compared to the nanoantennas and scatters a lot more light. This can also be seen on Figure 22. Since the particles are diffraction-limited, i.e. they are smaller than the illumination wavelength, the scattered signal is spread out over a point spread function (PSF). In order to collect as much information as possible, without including too much noise, an area is selected around the maximum intensity and the signal is averaged out over this area. When a dust particle is present in an array, the PSF of that particle will overlap substantially with the PSF of the nanoantennas since dust particles are generally bigger than the nanoantennas. The data for nanoantennas close to dust particles is therefore not used. This is done for the 2 measurements and the signal of the same nanoantenna is averaged out over the 2 measurements. The used EMCCD samples every 0.5 fs, corresponding to a sample rate of 2000 THz. Since the highest frequencies of interest are around 2 eV, or 483.6 THz, the sampling rate is well above the minimal sampling rate required by Nyquist [55]. The averaged out signal is subsequently Fourier transformed and the resonance frequency ω_{pl} and linewidth β_{pl} are retrieved from the spectrum in case of sole nanoantennas and Ω in case of strongly coupled antennas. The frequency of the rotating frame, ω_0 in Equation 30, is subtracted from the frequency axis. When a flat spectrum is obtained with variations less then 5%, there is no need for normalization. However, then the only relevant data is in the flat region. If the resonance of a nanoantenna falls out of this region, the data can not be properly analyzed.

5 Results

As described before, a coupled system consists of a plasmonic nanoantenna and molecules, and the properties of the coupled system are largely determined by the properties of both the components: the plasmonic and molecular resonance frequency ω_{pl} and ω_{mol}, the plasmonic and molecular linewidths β_{pl} and Γ_{mol}, the molecular transition dipole moment $\boldsymbol{\mu}$ and the field intensity and location of the hotspots of the nanoantennas. Therefore, measurements have to be carried out on both the molecules and nanoantennas before measuring the coupled systems.

Measurements on the molecules are carried out first. This way the molecular resonance frequency and the linewidth are determined and imported into the numerical simulations in order to obtain realistic results. Then, nanoantennas are measured in absence of molecules. From these measurements, ω_{pl} and β_{pl} are determined. If the results are satisfactory, meaning the results are consistent with the theoretical values, the molecules are added to the same sample and the coupled system is measured.

5.1 Molecules

First, the permittivity ϵ or equivalently the refractive index n of the LD800 is determined. This contains all the needed information, i.e. the resonance frequency ω_{mol} and the molecular linewidth Γ_{mol}. As mentioned before, ω_{mol} is an important to know parameter, since this is the frequency the nanoantennas are tuned to match as good as possible. Γ_{mol} is important for the distinction between weak and strong coupling.

To determine the permittivity ϵ, the absorbance A is measured using commercial ultraviolet-visible spectroscopy (UV-VIS) equipment with a quartz cuvette of 1 mm. The LD800 is diluted in ethanol to a concentration of 150 µM for the measurement, although the actual concentration will be different. The absorbance is defined as the logarithm of the transmitted power to the incident power of the sample [56]. The result of the measurement is shown in Figure 24, where the y-axis is expressed in arbitrary units. The absorbance spectrum has 2 clear peaks, at 1.82 eV and at 1.99 eV. However, only the peak with the highest amplitude is of interest since this peak will make coupling with the nanoantenna easier and stronger. The nanoantennas are therefore tuned to 1.82 eV. The imaginary part of the refractive index n_I is directly related to the absorbance and therefore has its main peak at 1.82 eV. In order to get useful information for numerical simulations out of this measurement, a Gaussian function is fitted over over the main peak of n_I. The fitted Gaussian has a FWHM of 0.116 eV.

In Section 2.1 it is mentioned that n_R and n_I are related to each other through the Kramers-Kronig equations. Assuming n_I is zero for all frequencies outside of the plot, n_R can be determined. Furthermore, using Equation 10, the complex permittivity is also known. n_R, ϵ_R and ϵ_I are calculated for the fitted Gaussian, since these functions are used for the numerical simulations and because the molecular linewidth Γ_{mol} corresponds to the FWHM of the peak in ϵ_I, which is also 0.116 eV.

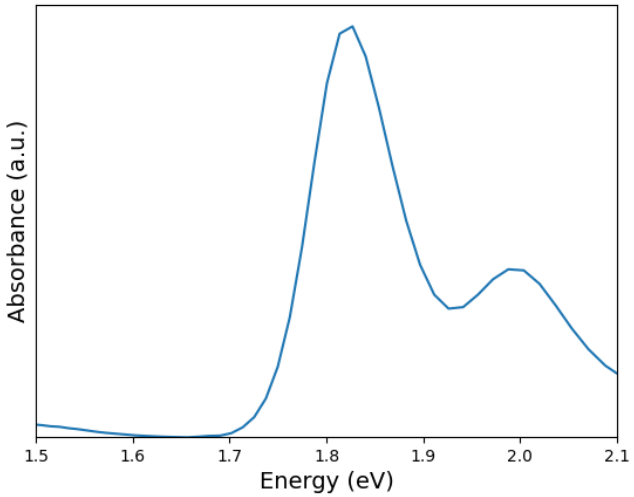

Figure 24: Absorbance of LD800

5.2 Nanoantennas

As described in Section 4.1, each sample consists of several arrays in which the length of the nanoantennas varies from 60 to 150 nm. Each sample has arrays with rods and arrays with dimers. The size of the gap in dimer arrays varies, even when this is not meant, but the length of nanoantennas is better controlled. Since the geometry of the rods only depends on the length and radius of curvature, it is good to look at the results of rods before looking at dimers. If the rods exhibit an offset in their resonance frequency from the theoretical values obtained in Section 3, several variations from the theoretical model can be the cause. The variations can be in the material constants, an offset in the length, the radius of curvature, or the roughness of the surface. This knowledge has to be taken into account when analyzing the measurements of the dimers. As mentioned before, the used setup produces a spectrum with a flat part. From Figure 23, it can be seen that the flat region ranges from 1.5 to 2.1 eV. Only the results in this region will be shown since it is the only relevant data.

A common problem with the data analysis is the error is alignment between the sample and the polarizer in the setup. If the sample is mounted somewhat tilted, some of the power from the source will excite the perpendicular mode. A tilting of 10° results in 3% of the power going into the perpendicular mode. From Figure 13 it is known that the perpendicular mode has a resonance frequency of 2.2 eV and from Figure 26a an offset of 0.1 eV can be expected. A peak between 2 and 2.1 eV appears in the scattering cross section of the nanoantennas consistently. To eliminate the influence of the perpendicular mode, a Lorentzian is fitted to the peak between 2 and 2.1 eV and is subtracted from the scattering cross section. The amplitude of the perpendicular mode is different for every measurement since the tilting angle of the sample is different every time the sample is mounted. So only if there is a peak present, it can be removed. If no peak is present, it is not possible to estimate the share of the perpendicular mode and the scattering cross section is not altered.

5.2.1 Rod antennas

First, the rod antennas are analyzed. As mentioned in Section 4.1, the length ranges from 60 to 150 nm with an increase of 10 nm. Figure 25 shows the measured scattering cross section of rods with lengths 60, 90, 120 and 150 nm. These rods are all located in the same array. The y-axis starts at 0 but has a different scale for the different plots. The first observation from the Figure is that the scattering spectrum is relatively uniform, both in the resonance energy and the intensity of the scattered field. Only in Figure 25a, 1 rod has a low quality. Another observation is that the off-resonance scattered field intensity for high energies is higher then for low energies. This is the result of Mie scattering.

Figure 26a compares the resonance energies from the measurements and the simulations of rods. There is a clear offset present. The resonance energy in experiment is lower in practice then in theory, but the offset is relatively consistent: $0.097 \pm 0.023\,\mathrm{eV}$. The offset and standard deviation are particularly low for the longer rods. However, this is due to the fact that only the part of the scattered field in the flat region of the laser spectrum is analyzed since data outside this region is not representative. The resonance of the longest rods lies most likely outside of this region. This is no problem since these rods and the dimers with the same length are no candidates for strong coupling anyway, their resonance energy is too far away from the molecular resonance. The reason for this offset can be an offset in the length of the rod, where the rod is longer than intended, or a lower radius of curvature.

Figure 26b compares β_{pl} for simulations and experiments. Here, the offset is not as consistent as for ω_{pl}, but β_{pl} is generally higher for the experiments. The offset is $0.048 \pm 0.030\,\mathrm{eV}$. This is the result from the inhomogeneity of the nanoantennas, coming from the fabrication process. The evaporation of Au on the sample results in a granular surface, while the nanoantennas in the simulations have a smooth surface. The granular surface intensifies electron-surface scattering, where an electron in the nanoantenna is deviated because of the rough surface and emits a photon. This photon can have a different frequency than the resonance frequency, therefore the peak will be broader [57]. Because the formation of the granular surface is different for every nanoantenna, the standard deviation is relatively high. β_{pl} still follows a certain trend, it decreases for increasing length of the nanoantenna, but it does not follow the simulated trend for the complete range.

5.2.2 Dimer antennas

Now that it is known that an offset in the resonance energy is to be expected, the dimers can be analyzed. Since the resolution of the used EBL equipment is 10 nm, variations in the gap and therefore in the scattering cross sections are expected for dimers. Therefore, the scattering cross sections of single nanoantennas will be examined, and not averaged out as for rods. An estimate can be made for the size of the gap by looking at the shift towards a lower frequency compared to the rod antenna with the same length, and comparing this shift

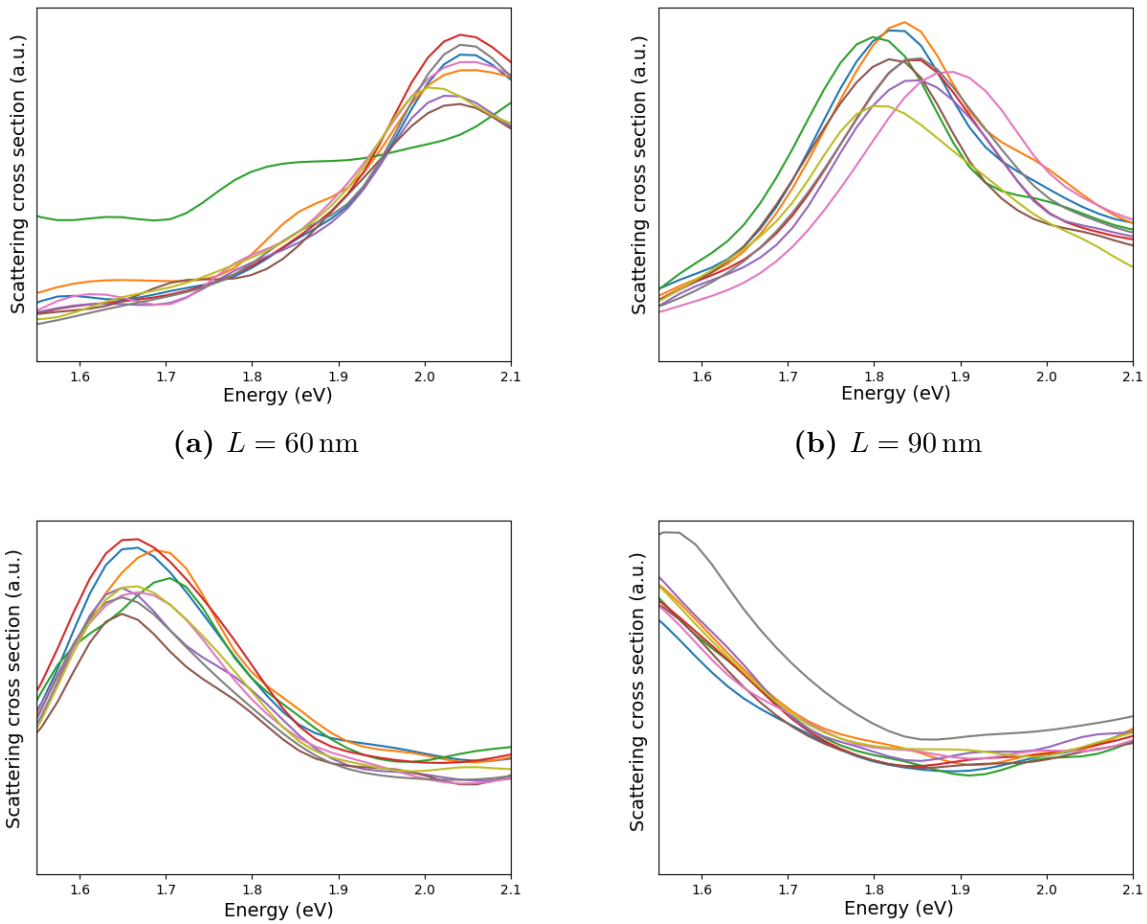

(a) $L = 60\,\mathrm{nm}$ **(b)** $L = 90\,\mathrm{nm}$

(c) $L = 120\,\mathrm{nm}$ **(d)** $L = 150\,\mathrm{nm}$

Figure 25: Results of scattering measurements of rods with different lengths

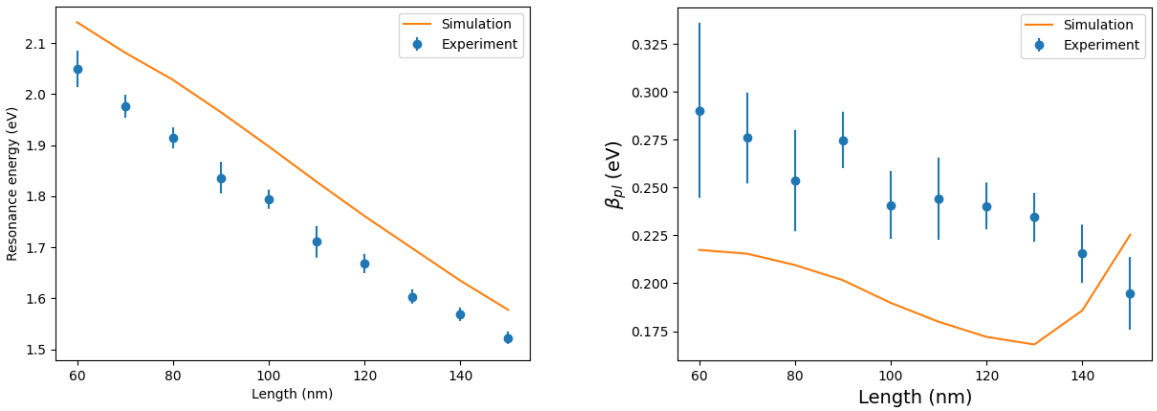

(a) Resonance energy ω_{pl} **(b)** Linewidth β_{pl}

Figure 26: Comparison between measured and simulated resonance energy and linewidth of rods

with the numerical simulations. This way, the offset of the rods is still taken into account. The discussion of the dimer nanoantennas will not be in detail, since it is more important to compare the cross sections with and without molecules. This will be done in Section 5.3.

The quality of the dimers is often worse then the quality of rods. The resonance of dimers does not always have the expected Lorentzian shape with a clear peak. Some dimers show a flat spectrum and have therefore no resonance at all in the expected area. Other dimers show 2 peaks of resonance. When molecules are added later, it is possible that the spectrum also shows 2 peaks, while strong coupling is not achieved. Some dimers also show a shoulder in their resonance peak. Dimers with no resonance or 2 resonances are therefore not useful for strong coupling. Because of the big variation in quality, only individual nanoantennas are examined and only the best ones are discussed. Also nanoantennas longer than 100 nm are not discussed in this section. In Figure 26a it can be seen that a 100 nm rod has a resonance frequency ω_{pl} of 1.8 eV, so a dimer will have a lower resonance frequency and on top of that, the presence of the molecules will further decrease the resonance frequency. This makes the mismatch with the molecular resonance frequency ω_{mol} too big.

As said in Section 4.1, samples have arrays with nanoantennas where the gap is intended to be 25 nm and where the gap is intended to be 30 nm. Variations in the gap are expected since the resolution of the EBL equipment is limited to 10 nm. Figure 27a and 27b each show the scattering cross section of 4 dimers with a length of 70 nm. In order to have a clear Figure, the scattering cross sections for the individual dimers have an offset. The depicted dimers have the best quality in their column. It is clear that the shape of the resonance is indeed distorted compared to the rods. The difference between the experimental resonance frequency of the dimer and the rods of 70 nm is calculated and the corresponding gap is determined and displayed on the legend in the figure. The experimental resonance frequency of 70 nm rods approximately matches the theoretical resonance frequency of 90 nm rods.

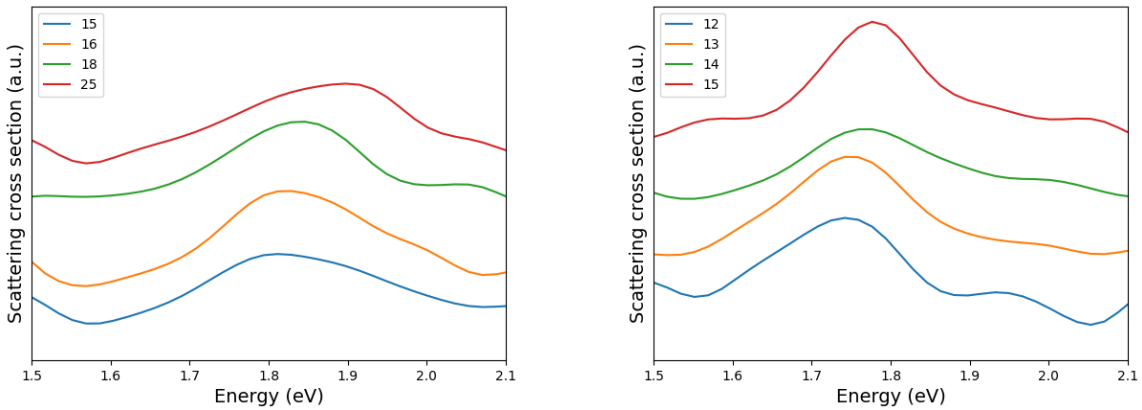

(a) Dimers with an intended gap of 30 nm **(b)** Dimers with an intended gap of 25 nm

Figure 27: Scattering cross section of dimers of 70 nm with different gaps

The determination of the gap is therefore done by comparing the theoretical shift of 90 nm nanoantennas. This method is only an estimate of the gap size since the length is not the only factor that influences ω_{pl}. Other reasons include an asymmetric dimer, different radii of curvature at different edges, the sides of the 2 rods not being flat inside the gap etc. For arrays with an intended gap of 25 nm, the gap ranges from 8 to 20 nm, while the range is from 13 to 27 nm for 30 nm gap arrays. The gap of 8 nm corresponds with an the smallest mode volume V_m, approximately 20 000 nm^3.

The resonance frequencies of the dimers in Figure 27a are between 1.8 and 1.9 eV. Taking into account that there will be a shift when adding molecules to the sample, these antennas are good candidates for strong coupling. The dimers in Figure 27b have resonances already below 1.8 eV and will have a bigger resonance mismatch. β_{pl} is remarkably higher than the expected values. In Figure 27a, the linewidth β_{pl} is 0.33, 0.33, 0.40 and 0.52 eV for the dimers with gaps 15, 16, 18 and 25 nm respectively. For Figure 27b, β_{pl} equals 0.26, 0.32, 0.44 and 0.37 eV for the 12, 13, 14 and 15 nm gap dimers respectively. Looking at the results for 90 nm dimers in Figure 10b, the difference in the experimental and theoretical β_{pl} is between 0 and 0.26 eV, while the difference for rods was only 0.048 eV on average. This again is a result of the worse quality of dimers compared to rods. The high values for β_{pl} make achieving strong coupling more challenging.

5.3 Nanoantennas and molecules

After measuring the sole nanoantennas, molecules are added on top of the same sample. This way, the scattering spectrum of the same nanoantenna with and without molecules can be compared. As mentioned before, it is important to measure shortly after adding the molecules. The molecular layer will evaporate, changing the molecular concentration from the intended concentration. Also dust particles may fall onto the sample.

Strong coupling is expected to happen with dimers, rather than with rods because dimers have a higher field intensity in their gap. On the other hand, β_{pl} is generally smaller for rods. Also the gap of a lot of dimers is relatively high, reducing the effect of the high field in the gap. Since the molecular concentration is relatively high, intended to be 150 mM, and the coupling strength is proportional to square root of the amount of molecules N, see Equation 20, strong coupling has been observed with both rods and dimers.

Strong coupling is detected by the presence of 2 peaks in the scattering cross section, the upper and lower polariton. But as said in the previous section, some nanoantennas show 2 peaks without molecules present. The coupled system therefore always has to be compared with the sole nanoantenna. To make sure that a system is really strongly coupled, neighbouring columns from the same array are also looked at. If the 2 peaks move towards the plasmonic and molecular resonance frequencies as described in Section 2.3.2, then the system exhibits anticrossing which confirms strong coupling.

In the next sections, the observed strong coupling will be discussed, both for rods and dimers. From the observed Rabi splitting, β_{pl} and ω_{pl} and knowledge about ω_{mol} and Γ_{mol}, the coupling strength g will be calculated and compared to $(\beta_{pl}+\Gamma_{mol})/4$, the minimal value for strong coupling.

5.3.1 Strong coupling with rod antennas

Rods with length 90 nm have an average resonance frequency ω_{pl} of 1.84 eV. This makes them a suitable candidate for strong coupling with a high molecular concentration, if they have a small enough linewidth β_{pl}. Figure 28 shows the rods where strong coupling is observed. On the left side, the scattering cross section of rods with molecules is shown, on the right side sole rods. In order to demonstrate the anticrossing behaviour, different lengths of the rods are shown, 100 and 110 nm. The scattering cross sections for different lengths are plotted with an offset in the y-axis and are normalized since longer nanoantennas have a higher scattering intensity. Also the absorbance spectra of LD800 is added as a reference. The colours on the left side match the colours on the right side in order to easily compare spectra.

Strong coupling is in fact only achieved for the 90 nm rods. The 100 and 110 nm have a too big resonance mismatch. The 2 peaks (or in some spectra 1 peak and a shoulder) coincide with the molecular resonance peak and the plasmonic resonance peak, confirming the anticrossing as shown in Figure 5. No useful measurement data is obtained for the 80 nm rods and they are therefore not included in Figure 28. As predicted by the numerical simulations, the presence of the molecules naturally decreases ω_{pl} and this can be seen well for the 100 and 110 nm nanoantennas. The shift varies from 0.08 eV to 0.12 eV, meaning the concentration is not uniform.

For the 90 nm rods the coupling strength g can be calculated, using Equation 25 and

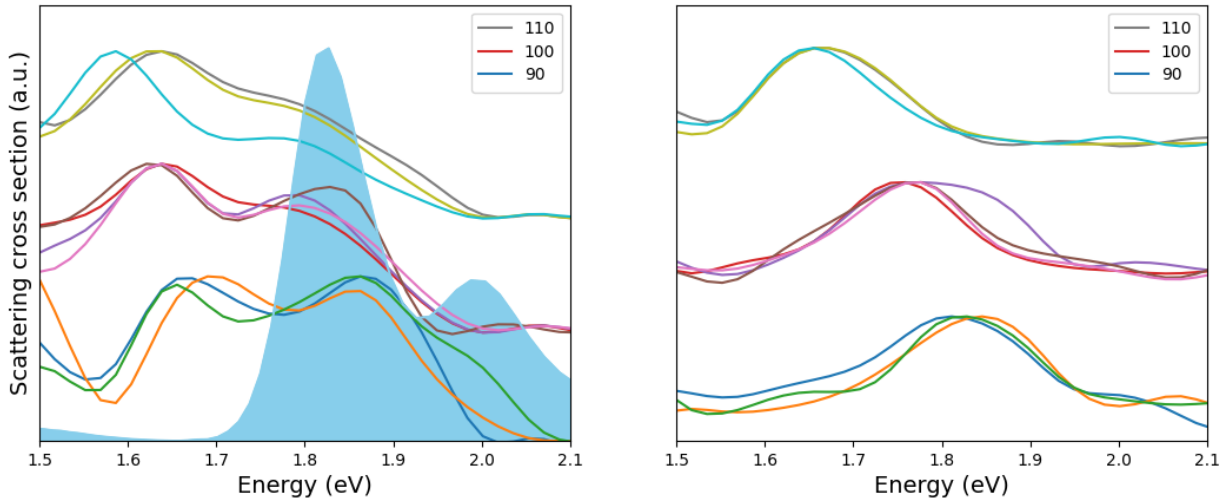

Figure 28: Comparison of scattering cross sections between (left) rods with molecules and (right) sole rods with matching colours. The absorbance of LD800 is added on the left. The lower band has a length of 90 nm, the middle one of 100 and the upper one of 110.

taking into account an estimated shift of 0.1 eV for ω_{pl}. For the blue, orange and green rods, g equals 0.099, 0.083 and 0.096 eV respectively, while $(\beta_{pl} + \Gamma_{mol})/4$ is 0.090, 0.082 and 0.081 eV respectively, confirming strong coupling. An estimate of the amount of molecules N will not be made for rods. To calculate N following Equation 21, the mode volume V_m has to be known. Unlike for dimers, determining the mode volume for rods is not trivial.

On another array with rods, strong coupling is achieved, but with 80 nm rods. The average coupling strength g for all the strongly coupled rods is 0.106 ± 0.017 eV, while the minimal value is 0.094 ± 0.011 eV.

5.3.2 Strong coupling with dimer antennas

With the rods, only 2 arrays had achieved strong coupling. For dimers, there are several, both because there are more arrays with dimers on a sample and because they are better suited. On the other hand, the quality of dimers is not as good as for the rods. The arrays with the best results will be discussed, the coupling strength g will be calculated and from the amount of interaction molecules N, the molecular concentration will be calculated by approximating V_m as the volume in the gap.

Figure 29 shows the results for dimers with lengths 70, 80 and 90 nm in an array with an intended gap of 30 nm. The variations in the gap cause dimers with equal lengths to have different resonance frequencies. The absorbance spectra is again included on the left side and the colours between the left and right side correspond to the same nanoantenna. As said in Section 5.2.2, the estimated gap can be as small as 15 nm. The gap decreases ω_{pl} and therefore, suitable dimers are shorter than rods.

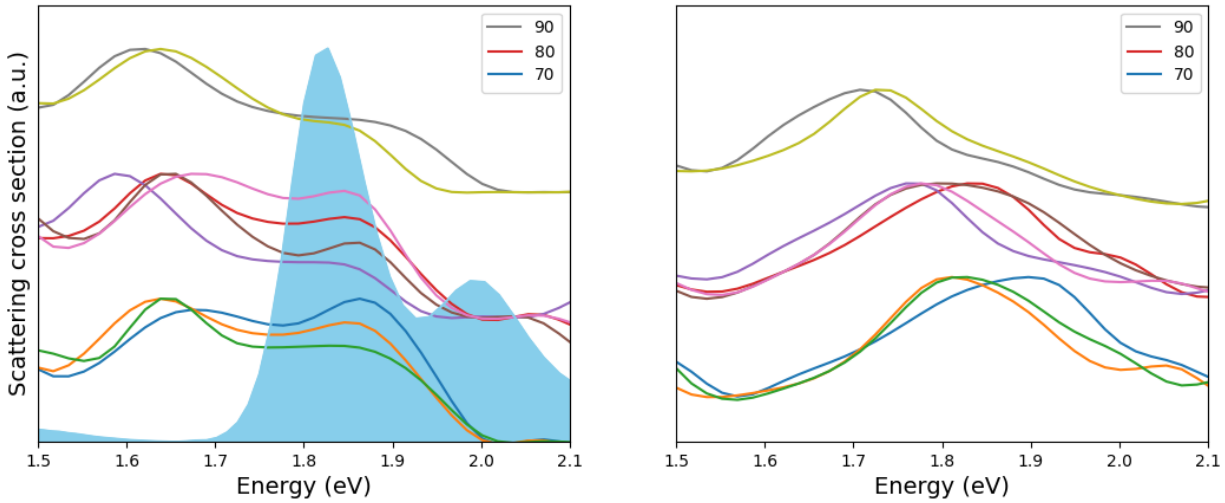

Figure 29: Comparison of scattering cross sections between (left) dimers with molecules and (right) sole dimers with matching colours in an array with gaps of 30 nm. The absorbance of LD800 is added on the left. The lower band has a length of 70 nm, the middle one of 80 and the upper one of 90.

Similarly as for the rod, the dimers that are off resonance with the molecules confirm anticrossing. These nanoantennas are used to estimate the natural shift in ω_{pl}. Here, the shift is 0.09 eV. Taking this into account, the coupling strength g is calculated and compared to $(\beta_{pl} + \Gamma_{mol})/4$ for the 70 nm nanoantennas. For the blue, orange and green nanoantennas, g equals 0.106, 0.098 and 0.103 eV while the minimal values are 0.105, 0.093 and 0.099 eV respectively, again confirming strong coupling.

The gap can be estimated for the dimers of 70 nm by comparing the shift to the simulations of 90 nm nanoantennas, as explained in Section 5.2.2. The intended gap in the array is 30 nm, the estimated gap is 30, 15 and 18 nm for the 3 dimers. Using Equation 21 and assuming that μ is parallel to the electric field, the obtained amount of molecules N is 7061, 3167 and 4153. This corresponds to a molecular concentration of 156, 140 and 153 mM if it is assumed that all the contributing molecules are located inside the gap. There is a non-negligible contribution in the coupling of the molecules outside the gap since also rods can achieve strong coupling, and not all the dipole moments will be aligned with the electric field. Therefore, the obtained values are only a rough estimate.

Figure 30 shows another array with strong coupling. The length of the dimers is 60, 70 and 80 nm. The intended gap is again 30 nm in this array. Both the dimers of 60 and 70 nm exhibit strong coupling. For the 60 nm antennas, g equals 0.113 ± 0.003 eV, every time above the minimal values 0.098 ± 0.007 eV. For the 70 nm dimers, g is 0.125 ± 0.008 eV, again above the minimal value 0.115 ± 0.001 eV. The 80 nm dimers are used to estimate the shift, here 0.19 eV on average. Also anticrossing is established, since the 80 nm dimers have a peak on

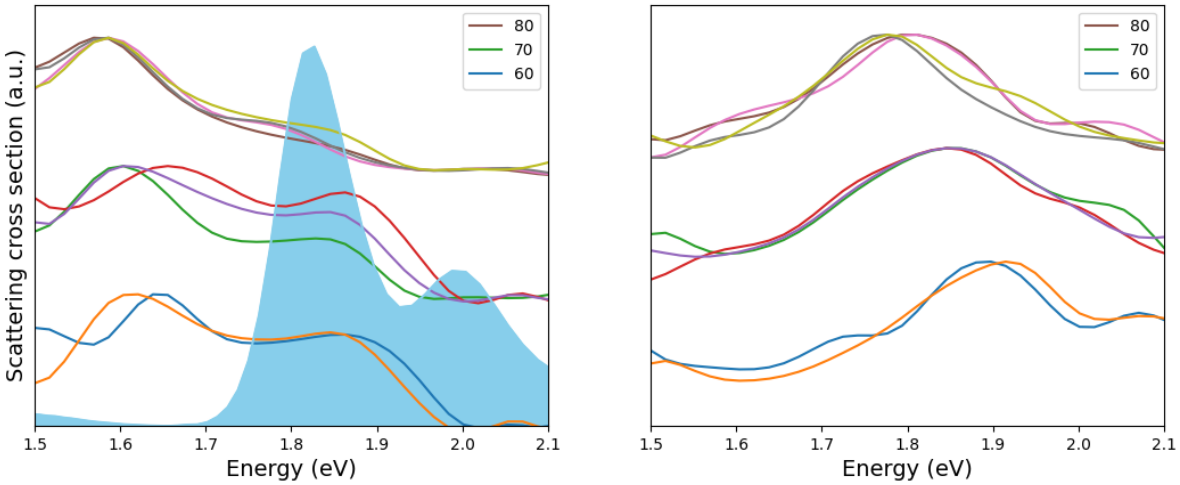

Figure 30: Comparison of scattering cross sections between (left) dimers with molecules and (right) sole dimers with matching colours in an array with gaps of 30 nm. The absorbance of LD800 is added on the left. The lower band has a length of 60 nm, the middle one of 70 and the upper one of 80.

their plasmonic resonance energy and a bump around the molecular resonance frequency.

At several other arrays strong coupling is observed (both Rabi splitting and anticrossing). Also with arrays with an intended gap of 25 nm. In Section 5.2.2, it is observed that at these arrays, ω_{pl} is already around 1.8 eV for 60 nm dimers. The natural decrease of ω_{pl} makes strong coupling harder to achieve than for arrays with 30 nm gaps. 65% of the observed strong coupling with dimers were in 30 nm gap arrays.

Taking into account all the dimers with strong coupling, the coupling strength g is 0.116 ± 0.014 eV with an minimal value of 0.103 ± 0.008 eV. This leads to an average molecular concentration of 195 ± 48 mM. The highest achieved coupling strength is 0.143 eV, with a 60 nm dimer with an estimated gap of 8 nm. g is on average 0.001 eV higher for 60 nm dimers. When comparing the amount of rods that achieved strong coupling to the amount of dimers, the dimers are 13% more likely to achieve strong coupling. Despite the higher minimal values for strong coupling (0.094 eV for rods, 0.103 eV for dimers), the field intensity in the gap still improves the probability of reaching strong coupling. No strong coupling is observed with the smaller absorption peak of LD800 at 1.99 eV.

5.4 Future work

It is clear that there is room for improvement in the experimental results. The fabrication of the nanoantennas can still be optimized by adjusting the dose of the EBL and also 50 nm dimers can be made to confirm anticrossing. To improve the quality of the gap and decrease the variations in the radius of curvature of the nanoantenna, other techniques can be employed. A good candidate for this is ion beam milling. The gap can then be controlled

down to 5 nm [58]. A nanoantenna is then grown with the same techniques as in this thesis, EBL and Au evaporation and the gap is cut out by an ion beam. Other designs can also be experimented with, the most obvious choices being the trimer and the Yagi-Uda nanoantenna. The trimer consists of 3 rods [59] and the Yagi-Uda nanoantenna is a row of rods with their long sides parallel to each other [60]. Other possibilities are the (inverse) bow-tie nanoantennas [61] or the nanoparticle-on-mirror (NPoM) design [43], although the NPoM design requires a different fabrication method.

Once the fabrication is optimized, the molecular concentration can be decreased, down to single molecules. The molecule would then have to be positioned inside the gap of the dimer. Different kind of molecules (with a different resonance frequency) can be experimented with as well by coupling them to nanoantennas with different lengths. When single-molecule strong coupling is achieved, the aforementioned applications become possible. The system then has to be built in in more complicated structures.

Other properties of the system can also be measured. In the first place, the Purcell factor F_P can be measured for the weakly coupled nanoantennas. The possibility of fluorescence in a strongly coupled system can be investigated, as well as the directionality of the scattered field.

6 Conclusions

From the theoretical background, numerical simulations and the measurement results, conclusions will be drawn in this section. The conclusions of the theory and the numerical FDTD simulations will be taken together since the simulations are a way of verifying the theoretical model and calculating exact values. The focus is on the measurement results.

6.1 Theory

The most important factor from the theoretical background is the coupling strength g, that allows distinction between 2 coupling regions, weak coupling and strong coupling. The magnitude of g depends on several factors: the molecular resonance frequency ω_{mol} and decay rate Γ_{mol}, the plasmonic resonance frequency ω_{pl} and linewidth β_{pl}, the transition dipole moment $\boldsymbol{\mu}$ and its relative orientation with the electric field produced by the nanoantenna, the magnitude of the electric field and the amount of molecules N. In order to get g as high as possible, ω_{pl} needs to be tuned to match ω_{mol}. 2 types of nanoantennas are investigated in this thesis: rods and dimers, where a dimer is 2 identical rods separated by a gap. The tuning of ω_{pl} can be done by varying the length and the gap size of the nanoantenna, where a longer length and a smaller gap cause a decrease of ω_{pl}. Dimers can create a higher field intensity than rods because they confine the electric field in the gap. Decreasing the gap increases the field intensity in the gap of the dimer. A higher field intensity leads to a higher value of g. ω_{pl} and β_{pl} are visible in the scattered field of a nanoantenna.

For small values of g, the system is in the weak coupling regime. The most important property of a weakly coupled system is the enhancement of the emission rate Γ_{mol} by the Purcell factor F_P. If g surpasses a minimal value, $(\beta_{pl}+\Gamma_{mol})/4$, strong coupling is achieved. The system then undergoes Rabi splitting. The scattering spectrum splits into 2 peaks, called the lower and upper polariton. They are separated by 2Ω or twice the Rabi frequency. Ω is the frequency with which energy is exchanged between molecules and nanoantenna and is also visible in the scattered field. From Ω, the coupling strength g can be retrieved. A dip in the scattering cross section appears at ω_{mol}, but the central frequency between the lower and upper polariton is $(\omega_{pl}+\omega_{mol})/2$. Due to the presence of the molecules, a natural shift towards lower frequencies in ω_{pl} occurs since ω_{pl} is dependent on the refractive index of the surrounding. If the plasmonic resonance frequency differs too much from the molecular resonance frequency, strong coupling can not be achieved. Generally, smaller gaps result in a stronger coupling because of their high electric field, as long as they don't make the mismatch in resonance between nanoantenna and molecule too big. If g is high enough to achieve strong coupling with a nanoantenna that is resonant with the molecules and other nanoantennas are not resonant because they have a different length, the upper and lower polariton converge to the plasmonic and molecular resonance frequencies without crossing each other. This is called anticrossing.

6.2 Measurements

From the measurements of the absorption spectrum of the molecules, 2 important conclusions can be drawn. The peak with the highest intensity corresponds to the molecular resonance frequency ω_{mol} and equals 1.82 eV. The linewidth of the peak is the emission rate Γ_{mol} and equals 0.116 eV.

The sole nanoantennas are measured before the molecules are added to the sample. This is done to know ω_{pl} and β_{pl}. So when the Rabi frequency Ω is measured, g can be calculated, as well as the minimal value for strong coupling.

A sample consists of several arrays with rods and arrays with dimers. 1 array has 10 columns and 9 rows, so 90 nanoantennas in total. The length of the nanoantennas ranges from 60 to 150 nm, corresponding with a 10 nm difference between 2 neighbouring columns. The measurements from the rods show that the resonance frequency ω_{pl} is 0.097 ± 0.023 eV lower then the simulated values, following the expected trend. β_{pl} is 0.048 ± 0.030 eV higher then the simulated values and largely follows the theoretical trend. The higher linewidth is the result of surface roughness that causes electron-surface scattering in the nanoantenna.

The gap in dimers can be estimated by comparing ω_{pl} for rods and dimers with the same length since the size of the gap determines the shift in ω_{pl}. The magnitude of the shift is compared with the simulated shifts and a gap is estimated. In arrays with an intended gap of 25 nm, the estimated gaps range from 8 nm to 20 nm, while for arrays with an intended gap of 30 nm, the range is between 13 nm and 27 nm. The mode volume V_m is approximated by the volume in the gap of a dimer. The smallest achieved mode volume is 20 000 nm^3 since the nanoantennas are 50 nm wide and high. Generally, β_{pl} is higher for dimers than for rods, matching the theoretical predictions. The quality of the dimers is on average worse than the quality of the rods. This means that some dimers show no peak in their scattered field at all in the expected region, or they show 2 peaks.

When ω_{pl} and β_{pl} are known, a solution of LD800 in ethanol is added to the sample and spin coated, resulting in a layer of 20 to 25 nm. The intended concentration is 150 mM, and from the measurement results an estimate of the concentration can also be made. If the scattering cross section of a nanoantenna with molecules shows 2 peaks and anticrossing is observed, strong coupling is reached. Even though a dimer has an advantage over rods to reach strong coupling because of the high field intensity in the gap, strong coupling has been observed with both rods and dimers.

In the case of rods, g is 0.106 ± 0.017 eV, while $(\beta_{pl} + \Gamma_{mol})/4$ is 0.094 ± 0.011 eV for 90 nm rods. For the dimers, g is 0.116 ± 0.014 eV, while $(\beta_{pl} + \Gamma_{mol})/4$ is 0.103 ± 0.008 eV. Strong coupling has been achieved with 60 nm and with 70 nm dimers. The estimated molecular concentration is 195 ± 48 mM. g is slightly higher for dimers than for rods. Comparing the amount of nanoantennas with strong coupling to the amount of nanoantennas on the sample, strong coupling is 13% more likely to happen at dimers.

The obtained results can still be optimized. The quality of the nanoantennas can be improved. For dimers, ion beam milling can be used to better control the gap. Furthermore, the molecular concentration can be decreased, down to single molecules. Different properties can be measured. The Purcell factor F_P can be determined for the weakly coupled nanoantennas, and the directionality of the scattered field as well. Also the possibility of fluorescence is a strongly coupled system can be investigated. Different nanoantennas, such as trimers or Yagi-Uda nanoantennas that both consists of rod antennas can be experimented with as well. With optimized nanoantennas and single molecule strong coupling, the system can be integrated in more complicated structures.

7 References

[1] J M Zhang and Y Liu. Fermi's golden rule: its derivation and breakdown by an ideal model. *European Journal of Physics*, 37(6):065406, oct 2016.

[2] James T Hugall, Anshuman Singh, and Niek F van Hulst. Plasmonic cavity coupling. *Acs Photonics*, 5(1):43–53, 2018.

[3] Lars Kastrup and Stefan W Hell. Absolute optical cross section of individual fluorescent molecules. *Angewandte Chemie International Edition*, 43(48):6646–6649, 2004.

[4] David Pines and David Bohm. A collective description of electron interactions: Ii. collective vs individual particle aspects of the interactions. *Physical Review*, 85(2):338, 1952.

[5] En Cao, Weihua Lin, Mengtao Sun, Wenjie Liang, and Yuzhi Song. Exciton-plasmon coupling interactions: from principle to applications. *Nanophotonics*, 7(1):145–167, 2018.

[6] Liang Tang, Sukru Ekin Kocabas, Salman Latif, Ali K Okyay, Dany-Sebastien Ly-Gagnon, Krishna C Saraswat, and David AB Miller. Nanometre-scale germanium photodetector enhanced by a near-infrared dipole antenna. *Nature Photonics*, 2(4):226–229, 2008.

[7] Ximei Qian, Xiang-Hong Peng, Dominic O Ansari, Qiqin Yin-Goen, Georgia Z Chen, Dong M Shin, Lily Yang, Andrew N Young, May D Wang, and Shuming Nie. In vivo tumor targeting and spectroscopic detection with surface-enhanced raman nanoparticle tags. *Nature biotechnology*, 26(1):83–90, 2008.

[8] Päivi Törmä and William L Barnes. Strong coupling between surface plasmon polaritons and emitters: a review. *Reports on Progress in Physics*, 78(1):013901, 2014.

[9] Ora Bitton, Satyendra Nath Gupta, and Gilad Haran. Quantum dot plasmonics: from weak to strong coupling. *Nanophotonics*, 8(4):559–575, 2019.

[10] Changsuk Noh. Emission of single photons in the weak coupling regime of the jaynes cummings model. *Scientific Reports*, 10(1):1–8, 2020.

[11] H Jeff Kimble. The quantum internet. *Nature*, 453(7198):1023–1030, 2008.

[12] Changlong Wang and Didier Astruc. Nanogold plasmonic photocatalysis for organic synthesis and clean energy conversion. *Chemical Society Reviews*, 43(20):7188–7216, 2014.

[13] Simanta Kundu and Amitava Patra. Nanoscale strategies for light harvesting. *Chemical reviews*, 117(2):712–757, 2017.

[14] John David Jackson. Classical electrodynamics, 1999.

[15] WL Bade. Drude-model calculation of dispersion forces. i. general theory. *The Journal of Chemical Physics*, 27(6):1280–1284, 1957.

[16] Colin Warwick and Signal Integrity Product. Keysight technologies understanding the kramers-kronig relation using a pictorial proof. *Physical Review*, 104:1760–1770, 1956.

[17] Peter B Johnson and R-WJPrB Christy. Optical constants of the noble metals. *Physical review B*, 6(12):4370, 1972.

[18] Pablo G Etchegoin, EC Le Ru, and M Meyer. An analytic model for the optical properties of gold. *The Journal of chemical physics*, 125(16):164705, 2006.

[19] Mai Sallam, Guy Vandenbosch, Georges Gielen, and Ezzeldin Soliman. Integral equations formulation of plasmonic transmission lines. *Optics Express*, 22:22388–22402, 09 2014.

[20] Ahmad Mohammadi, Vahid Sandoghdar, and Mario Agio. Gold, copper, silver and aluminum nanoantennas to enhance spontaneous emission. *Journal of Computational and Theoretical Nanoscience*, 6(9):2024–2030, 2009.

[21] Craig F Bohren and Donald R Huffman. *Absorption and scattering of light by small particles*. John Wiley & Sons, 2008.

[22] Fei Zhou, Zhi-Yuan Li, Ye Liu, and Younan Xia. Quantitative analysis of dipole and quadrupole excitation in the surface plasmon resonance of metal nanoparticles. *The Journal of Physical Chemistry C*, 112(51):20233–20240, 2008.

[23] Jorge Zuloaga and Peter Nordlander. On the energy shift between near-field and far-field peak intensities in localized plasmon systems. *Nano letters*, 11(3):1280–1283, 2011.

[24] Min Hu, Carolina Novo, Alison Funston, Haining Wang, Hristina Staleva, Shengli Zou, Paul Mulvaney, Younan Xia, and Gregory V Hartland. Dark-field microscopy studies of single metal nanoparticles: understanding the factors that influence the linewidth of the localized surface plasmon resonance. *Journal of materials chemistry*, 18(17):1949–1960, 2008.

[25] Michael Quinten. *Optical properties of nanoparticle systems: Mie and beyond*. John Wiley & Sons, 2010.

[26] Warren J Wiscombe. Improved mie scattering algorithms. *Applied optics*, 19(9):1505–1509, 1980.

[27] P Alonso-González, P Albella, M Schnell, J Chen, F Huth, A García-Etxarri, F Casanova, F Golmar, L Arzubiaga, LE Hueso, et al. Resolving the electromagnetic mechanism of surface-enhanced light scattering at single hot spots. *Nature communications*, 3(1):1–7, 2012.

[28] Kyle D Osberg, Nadine Harris, Tuncay Ozel, Jessie C Ku, George C Schatz, and Chad A Mirkin. Systematic study of antibonding modes in gold nanorod dimers and trimers. *Nano letters*, 14(12):6949–6954, 2014.

[29] E Prodan and PJCP Nordlander. Plasmon hybridization in spherical nanoparticles. *The Journal of chemical physics*, 120(11):5444–5454, 2004.

[30] Dmitri K Gramotnev and Sergey I Bozhevolnyi. Plasmonics beyond the diffraction limit. *Nature photonics*, 4(2):83–91, 2010.

[31] Lukas Novotny and Niek Van Hulst. Antennas for light. *Nature photonics*, 5(2):83–90, 2011.

[32] Kurt E Oughstun and Natalie A Cartwright. On the lorentz-lorenz formula and the lorentz model of dielectric dispersion. *Optics express*, 11(13):1541–1546, 2003.

[33] K Licha and Ute Resch-Genger. Fluorescent reporters and optical probes. In *Comprehensive biomedical physics*, pages Chapter–4. Elsevier, 2014.

[34] Denis G Baranov, Martin Wersall, Jorge Cuadra, Tomasz J Antosiewicz, and Timur Shegai. Novel nanostructures and materials for strong light–matter interactions. *Acs Photonics*, 5(1):24–42, 2018.

[35] F.J. Duarte and A. Costela. Lasers — dye lasers. In Robert D. Guenther, editor, *Encyclopedia of Modern Optics*, pages 400–414. Elsevier, Oxford, 2005.

[36] Kerry J Vahala. Optical microcavities. *nature*, 424(6950):839–846, 2003.

[37] Edward Mills Purcell. Spontaneous emission probabilities at radio frequencies. In *Confined electrons and photons*, pages 839–839. Springer, 1995.

[38] Stefan A Maier. Plasmonic field enhancement and sers in the effective mode volume picture. *Optics Express*, 14(5):1957–1964, 2006.

[39] Emilie Wientjes, Jan Renger, Alberto G Curto, Richard Cogdell, and Niek F Van Hulst. Strong antenna-enhanced fluorescence of a single light-harvesting complex shows photon antibunching. *Nature communications*, 5(1):1–7, 2014.

[40] Elad Eizner, Ori Avayu, Ran Ditcovski, and Tal Ellenbogen. Aluminum nanoantenna complexes for strong coupling between excitons and localized surface plasmons. *Nano letters*, 15(9):6215–6221, 2015.

[41] Bruce W Shore and Peter L Knight. The jaynes-cummings model. *Journal of Modern Optics*, 40(7):1195–1238, 1993.

[42] Peter L Knight and Peter W Milonni. The rabi frequency in optical spectra. *Physics Reports*, 66(2):21–107, 1980.

[43] Rohit Chikkaraddy, Bart De Nijs, Felix Benz, Steven J Barrow, Oren A Scherman, Edina Rosta, Angela Demetriadou, Peter Fox, Ortwin Hess, and Jeremy J Baumberg. Single-molecule strong coupling at room temperature in plasmonic nanocavities. *Nature*, 535(7610):127–130, 2016.

[44] Lukas Novotny. Strong coupling, energy splitting, and level crossings: A classical perspective. *American Journal of Physics*, 78(11):1199–1202, 2010.

[45] Jason McKeever, Andreea Boca, A David Boozer, Joseph R Buck, and H Jeff Kimble. Experimental realization of a one-atom laser in the regime of strong coupling. *Nature*, 425(6955):268–271, 2003.

[46] Perry R Rice and HJ Carmichael. Photon statistics of a cavity-qed laser: A comment on the laser–phase-transition analogy. *Physical Review A*, 50(5):4318, 1994.

[47] Stephen E Harris, JE Field, and A Imamoğlu. Nonlinear optical processes using electromagnetically induced transparency. *Physical Review Letters*, 64(10):1107, 1990.

[48] Tatjana Wilk, Simon C Webster, Axel Kuhn, and Gerhard Rempe. Single-atom single-photon quantum interface. *Science*, 317(5837):488–490, 2007.

[49] Stefan A Maier. Effective mode volume of nanoscale plasmon cavities. *Optical and Quantum Electronics*, 38(1):257–267, 2006.

[50] Eyal Feigenbaum and Meir Orenstein. Optical 3d cavity modes below the diffraction-limit using slow-wave surface-plasmon-polaritons. *Optics express*, 15(5):2607–2612, 2007.

[51] RFW Pease. Electron beam lithography. *Contemporary Physics*, 22(3):265–290, 1981.

[52] Vitor R Manfrinato, Fernando E Camino, Aaron Stein, Lihua Zhang, Ming Lu, Eric A Stach, and Charles T Black. Patterning si at the 1 nm length scale with aberration-corrected electron-beam lithography: tuning of plasmonic properties by design. *Advanced Functional Materials*, 29(52):1903429, 2019.

[53] Guy Cox and Colin JR Sheppard. Practical limits of resolution in confocal and non-linear microscopy. *Microscopy research and technique*, 63(1):18–22, 2004.

[54] Matz Liebel, Costanza Toninelli, and Niek F van Hulst. Room-temperature ultrafast nonlinear spectroscopy of a single molecule. *Nature Photonics*, 12(1):45–49, 2018.

[55] HJ Landau. Sampling, data transmission, and the nyquist rate. *Proceedings of the IEEE*, 55(10):1701–1706, 1967.

[56] Chuanmin Hu, Frank E Muller-Karger, and Richard G Zepp. Absorbance, absorption coefficient, and apparent quantum yield: A comment on common ambiguity in the use of these optical concepts. *Limnology and Oceanography*, 47(4):1261–1267, 2002.

[57] VA Gasparov and R Huguenin. Electron-phonon, electron-electron and electron-surface scattering in metals from ballistic effects. *Advances in Physics*, 42(4):393–521, 1993.

[58] Frances I Allen, Nathan R Velez, Rachel C Thayer, Nipam H Patel, Mary Ann Jones, Gregory F Meyers, and Andrew M Minor. Gallium, neon and helium focused ion beam milling of thin films demonstrated for polymeric materials: study of implantation artifacts. *Nanoscale*, 11(3):1403–1409, 2019.

[59] Hancong Wang. Plasmonic refractive index sensing using strongly coupled metal nanoantennas: nonlocal limitations. *Scientific reports*, 8(1):1–8, 2018.

[60] Ivan S Maksymov, Isabelle Staude, Andrey E Miroshnichenko, and Yuri S Kivshar. Optical yagi-uda nanoantennas. *Nanophotonics*, 1(1):65–81, 2012.

[61] Víctor Pacheco-Peña, Miguel Beruete, Antonio I Fernández-Domínguez, Yu Luo, and Miguel Navarro-Cía. Description of bow-tie nanoantennas excited by localized emitters using conformal transformation. *Acs Photonics*, 3(7):1223–1232, 2016.